JOURNAL OF GEOPHYSICAL RESEARCH, VOL. 115, B03408, doi:10.1029/2009JB006361, 2010

Quantitative description and analysis of earthquake-induced deformation zones along strike-slip and dip-slip faults

Wen-Jeng Huang[1,2] and Arvid M. Johnson[1]

Received 6 February 2009; revised 9 August 2009; accepted 21 September 2009; published 16 March 2010.

[1] Deformation zones are belts of high strains that can occur at the ground surface centered or asymmetrical relative to the trace of an earthquake fault and can range in width from a meter or two up to hundreds of meters. In order to minimize damage to engineering structures within deformation zones one needs to be able to determine the characteristics of the deformation zones. We develop an elastic-plastic model of fault slip propagation to explain formation of deformation zones and estimate certain parameters to characterize deformation zones. Our theory suggests the ratio of widths of deformation zones in hanging wall and footwall of dipping faults should be controlled by fault dip angle and the kind of fault; the relations are different for strike-slip and dip-slip faults. Also, the total width of the deformation zone normalized with fault slip during the earthquake should be determined by the dip angle, the exponent of the yield condition, and the kind of fault. The theoretical parameters measured for deformation zones along the strike-slip Düzce-Bolu fault at Kaynaşlı, Turkey, and two deformation zones along the Chi-Chi thrust fault, Taiwan, agree well with parameters determined from geophysical and geological sources. The theoretical model also indicates that the Winnetka strain belts related to the 1994 Northridge earthquake could have formed above a previously unknown blind fault at Winnetka; the analysis suggests that the Winnetka fault is a normal, dip-slip fault, dipping ~54°S with a fault tip depth of ~360 m.

Citation: Huang, W.-J., and A. M. Johnson (2010), Quantitative description and analysis of earthquake-induced deformation zones along strike-slip and dip-slip faults, *J. Geophys. Res.*, *115*, B03408, doi:10.1029/2009JB006361.

1. Introduction

[2] It is unquestionable in the earthquake engineering and geoscience communities that earthquakes cause damage to engineering structures by ground shaking and various kinds of foundation soil failures even far from the hypocenter and the earthquake rupture, but it is generally unappreciated that much of the damage to near-fault engineering structures can be due to two other distinctly different earthquake phenomena: seismic pulses of ground on the one hand and distortion of ground on the other [*Gür*, 2004]. Seismic pulses and distortion are quite distinct from ground shaking although they can all occur together. Seismic pulses and shaking are both essentially dynamic. The ground shaking is relatively easy to be accepted and understood because of its distinct nature. Seismic pulsing is a phenomenon where the ground lurches even a meter or more unidirectionally within a few seconds, causing sudden, high, ground velocities and concomitant accelerations during the earthquake if the earthquake rupture reaches the ground surface. The phenomenon was observed in recent years after strong motion stations were arranged near earthquake fault traces. In ground distortion, the ground is strained or fractured within a belt at the earth's surface due to faulting. It can be either dynamic, associated with sudden earthquake faulting, or static, associated with slow, "silent" faulting. In this paper we focus on ground distortion.

[3] Several geologists, G. K. Gilbert, F. E. Matthes, E. S. Larsen and A. Lawson, who were charged with describing the rupture of the 1906 San Francisco earthquake mostly north of San Francisco, showed incontrovertibly that earthquake ruptures were in some cases traces of fault planes but in many cases were zones of distortion [*Lawson*, 1908; *Reid*, 1910], which we now call *deformation zones*. Deformation zones and belts range in width from a few meters to half a kilometer along strike-slip earthquake ruptures at Landers, California, and Kaynaşlı, Turkey [*Johnson et al.*, 1994a, 1994b, 1997, 2002; *Fleming and Johnson*, 1997; *Fleming et al.*, 1997]. The idea of the deformation belts or deformation zones is analogous to the ideas of "fault zones" [e.g., *Gamond*, 1983], "process zones" [e.g., *Atkinson*, 1987; *Vermilye and Scholz*, 1998], "shear belts," or "fracture belts" [e.g., *Johnson et al.*, 1994a, 2002].

[4] Although some engineers have recognized that deformation zones with large strains can seriously damage engineering structures [e.g., *Steinbrugge et al.*, 1973; *Lazarte et al.*, 1994; *Gür*, 2004; Taiwan National Center for Research on Earthquake Engineering (NCREE), 921 Chi-Chi earthquake database analysis and management system (in Chinese), 2000, available at http://gisdb.ncree.gov.tw/ncree/doc/,

[1]Department of Earth and Atmospheric Sciences, Purdue University, West Lafayette, Indiana, USA.
[2]Now at Institute of Earth Sciences, Academia Sinica, Taipei, Taiwan.

0148-0227/10/2009JB006361

hereafter cited as NCREE, online database, 2000], the causes of deformation zones have remained obscure. The purpose of this paper is to describe and then analyze quantitatively the phenomena of ground distortion in deformation zones along several earthquake ruptures as a step toward developing an understanding of the causes of deformation zones. Engineers ultimately need to have quantitative information about how, why and where deformation zones occur in order to design engineering structures to appropriately address them.

[5] The proposed mechanism is based on the proposition that deformation zones form as slip on a fault propagates toward the ground surface. The proposition evolved out of studies of deformation zones along strike-slip earthquake ruptures in California and Turkey [*Johnson et al.*, 1993, 1994a, 1994b, 1996a, 1996b, 1997, 2002; *Fleming and Johnson*, 1997; *Fleming et al.*, 1997, 1998] and of growth of ruptures bounding large, rapidly moving landslide masses in Utah [*Fleming and Johnson*, 1989].

[6] The theoretical analysis formulated here quantifies the mechanism approximately and suggests physical properties of the ground, geometrical properties of the fault, and kinematic properties of slip on the fault that control the ways ideal deformation zones manifest themselves. Then we summarize field descriptions of deformation zones along two surface ruptures (Düzce-Bolu strike-slip fault at Kaynaşlı, Turkey [*Johnson et al.*, 2002], and the Chi-Chi thrust fault in Taiwan [*Huang*, 2006]), as well as a deformation zone over the Winnetka blind fault at Northridge, California [*Cruikshank et al.*, 1996], and use the theoretical analysis to compare values of parameters measured in the field with values of parameters expected theoretically. We note that the name Chi-Chi thrust fault is used instead of Chelungpu thrust fault for the fault that reactivated during the 1999 Chi-Chi earthquake, as largely accepted by geologists and geophysicists, because the Chi-Chi earthquake rupture did not everywhere occur along the surface trace of Chelungpu fault.

2. How Deformation Zones Develop

[7] The mechanism of deformation zone development that *Johnson et al.* [2002] have proposed is based essentially on three ideas borne of observation. First, the deformation zone is characterized by permanent deformation at the ground surface: fracturing or some kind of flow. Second, the general nature of the deformation in the zone is consistent with the slip on the fault that produces the zone. A corollary is that the deformation in the zone is opposite to that of elastic rebound. Third, the deformation zone forms as slip on a fault propagates toward the ground surface. A corollary is that a deformation zone forms before the slip on the fault reaches the ground surface. Although the mechanism of deformation zone formation has been developed for strike-slip faults [*Johnson et al.*, 2002], it is clear that the general mechanism should apply to deformation zones associated with dip-slip faults.

[8] The characteristic permanent deformations in deformation zones are manifested in different ways. Along the Johnson Valley and Homestead Valley fault zones at Landers, the ground was brittle and the interiors of the deformation zones were marked by spectacular arrays of small faults and tension cracks [*Johnson et al.*, 1993, 1994b, 1996b]. Along the northern part of the Emerson Lake fault zone at Landers, the soils were soft and sandy and, although the deformation zones could be recognized and the main rupture easily recognized, the internal deformation was mainly by flow so that rupturing was visible in only a few small faults and tension cracks [*Fleming and Johnson*, 1997; *Fleming et al.*, 1997; *Johnson et al.*, 1996b]. At Kaynaşlı, Turkey, the earthquake rupture passed through alluvium, so only the main rupture and a couple of other fractures were recognized [*Johnson et al.*, 2002]. The full width of the deformation zone was detected only by measuring displacements of piers supporting the Kaynaşlı Viaduct and calculating ground strains [*Johnson et al.*, 2002; *Gür*, 2004].

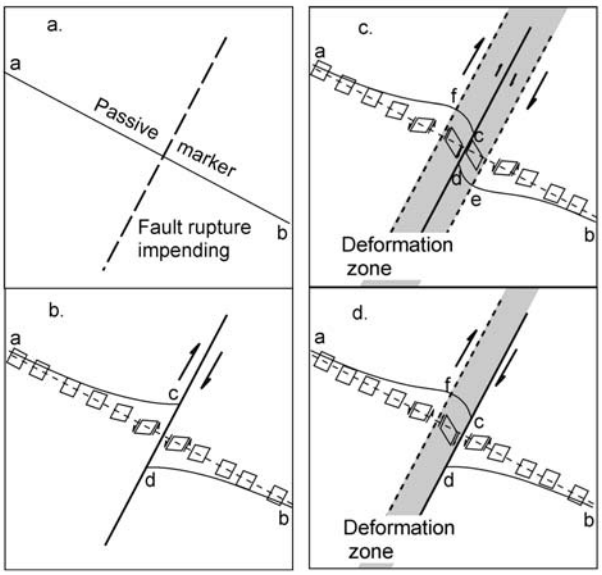

Figure 1. Idealized ground deformation along earthquake ruptures with pure right-lateral strike slip for a fault of finite length [after *Johnson et al.*, 2002]. The senses of distortion are indicated via exaggerated deformation of squares into parallelograms. (a) Map view of the trace of a strike-slip fault (dashed line). Passive marker, ab, placed across the area just prior to earthquake rupturing. (b) Essence of classic elastic rebound theory [*Reid*, 1910]. Note that the offset on the fault is right lateral but the deformed line and passive squares indicate that the rock on either side of the fault was distorted in a left-lateral sense as a result of elastic rebound. The sense of shearing in rebound is illustrated via the exaggerated deformation of squares into parallelograms on either side of the fault. (c) A zone of permanent right-lateral deformation. The deformation zone includes the right-lateral fault and is bounded on either side by elastic rebound that dies off with distance from a fault of finite length. Initial conditions were the same as in Figure 1a, but a deformation zone, a zone of permanent right-lateral deformation, straddles the main right-lateral rupture on which the slip propagated to the ground surface (in mode III). (d) Same as Figure 1c but the main rupture is near one side of deformation zone.

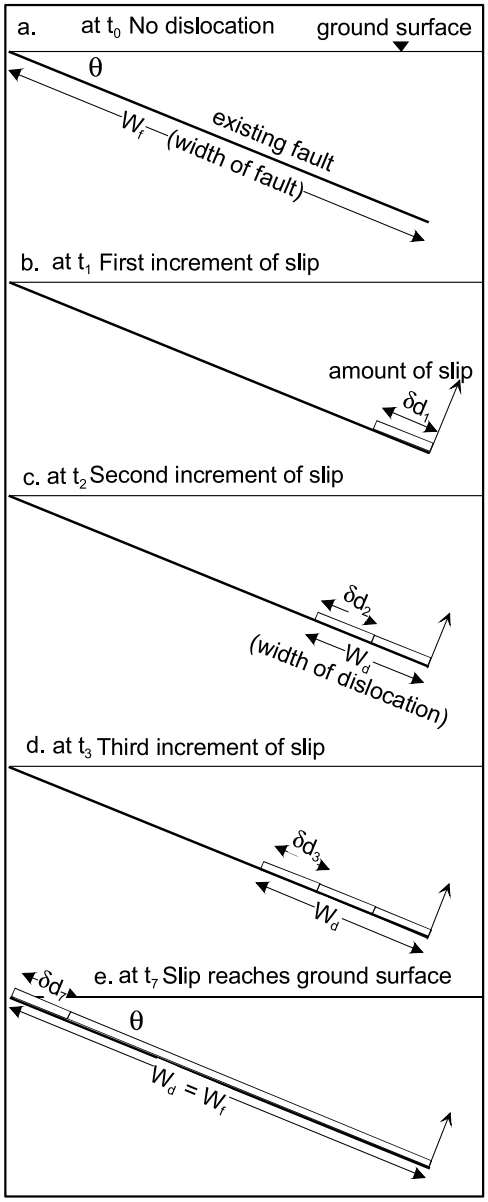

Figure 2. Simulation of propagation of uniform slip toward the ground surface along an existing fault. Slip is zero in front of tip of the slipped patch. Slip is uniform along slipped part of fault. (a) Cross section of fault of width, W_f, dipping at $\theta = 30°$. (b) At time t_1, first increment of dislocation of width δd_1 slips a certain amount. (c) At time t_2, a second dislocation with the same width is added in front of the first, making the total width of the dislocation $\delta d_1 + \delta d_2 = W_d$. The slip, though, remains the same for δd_1, δd_2, and W_d. (d) Another dislocation with the same width is added to the first two $\delta d_1 + \delta d_2 + \delta d_3 = W_d$. (e) Four more incremental dislocations added sequentially until the slip reaches the ground surface and $W_d = W_f$. The slip is finally uniform over the width of the fault, W_f.

[9] According to elementary elastic rebound theory [e.g., *Gilbert*, 1907; *Reid*, 1910], the phenomena illustrated in Figures 1a and 1b will occur at the ground surface for a right-lateral, strike-slip fault of finite length if a straight passive marker is placed normal to the trace of the fault (Figure 1a) shortly before the fault ruptures. When the fault slips suddenly at depth, the passive marker is offset and will deform as shown schematically in Figure 1b. The critical observation here is that elastic strains that accumulated in the ground prior to placement of the passive marker are released by the faulting. Thus the right-lateral offset on the fault produces left-lateral shearing deformation in ground on either side of the fault, and the passive marker, at the ground surface, indicates the left-lateral shearing. This is the result of elastic rebound. The rebound is illustrated via the exaggerated deformation of squares into parallelograms on either side of the fault.

[10] A deformation zone, however, is characterized by a distinctly different pattern of deformation of the passive marker (Figure 1c). If offset on the fault is right-lateral, then the sense of shearing within the deformation zone is also right lateral. On either side of the deformation zone, however, the deformation is left lateral, reflecting elastic rebound. In effect, the deformation zone and the main fault together accomplish the faulting near the ground surface that may well be accomplished on a single fault surface at depth. Two idealized versions of the position of the main fault with respect to the deformation zone are shown in Figures 1c and 1d. In both versions, however, the initial condition is the same as that for elastic rebound, shown in Figure 1a. The position of the main fault in Figure 1c is near midwidth so it appears to be similar to the position of the main fault at the San Andreas Reservoir intake structure [*Lawson*, 1908, Figure 35, p. 98]. The position in Figure 1d is closer to one side of the deformation zone so it appears to be similar to the position of the main rupture at Kaynaşlı, Turkey [*Johnson et al.*, 2002].

[11] The third idea underlying the mechanism proposed for the formation of deformation zones derives from the field observations that fault slip propagation near the ground surface (i.e., within the part of the ground that affects the formation of deformation zones) is upward for strike-slip faults. In particular, the surficial expressions of strike-slip ruptures that have been observed in large landslides in Utah [*Fleming and Johnson*, 1989], the 1989 Loma Prieta earthquake ruptures [*Aydin et al.*, 1992; *Martosudarmo et al.*, 1996], the 1992 Landers earthquake [e.g., *Johnson et al.*, 1994b, 1996b] and the 1999 Kaynaşlı, Turkey, earthquake [*Johnson et al.*, 2002]: all reflect mode III propagation, that is, propagation of faults from below to the ground surface. One reason we know that strike-slip fault segments could not have been propagating near the ground surface in mode II is that the traces of segments are discontinuous at the ground surface; mode II propagation would require continuity. The segments must have been propagating in mode III. For strike-slip faults, therefore, we would expect stresses induced by mode III loading to control the patterns of the near-surface strains and fracturing in the deformation zones. That is what we have deduced in all above mentioned studies of fractures within strike-slip deformation zones. We have few observations about direction of propagation of dip-slip faults near the ground surface. We will assume that the traditional view prevails, that dip-slip faults propagate in mode II near the ground surface.

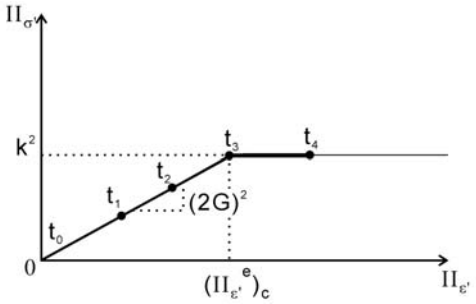

Figure 3. Relation between second invariants of deviatoric stress, $II_{\sigma'}$, and deviatoric strain, $II_{\varepsilon'}$ for elastic-plastic material. Deformation path is for continuous loading of the elastic-plastic material at a point on the ground surface. At four time steps, four dislocations are added to the idealized fault, as in Figure 2. The slope of the relation between invariants $II_{\sigma'}$ and $II_{\varepsilon'}^{e}$ is proportional to the square of twice the shear modulus, G. The relation is linear for times, t_1, t_2, t_3, as three incremental dislocations are added because the loading is within the elastic range. Yielding is impending at time t_3; the second invariant of deviatoric stress is at the critical value $(II_{\sigma'})_c = k^2$, where k is yield strength, and the second invariant of deviatoric elastic strains is at its critical value also, $(II_{\varepsilon'}^{e})_c = (k/2G)$. With continued loading between times t_3 and t_4, $II_{\sigma'}$ remains equal to k^2, whereas the total strain invariant, $II_{\varepsilon'}$, increases because it includes both elastic and plastic strains and exceeds $(II_{\varepsilon'}^{e})_c$.

[12] Deformation zones begin to form at the ground surface before the *slip front* on the fault reaches the ground surface. That is, the tip of propagation is "blind" at the time the deformation zone forms at the ground surface. The highly localized, intense shearing that we call the fault trace only occurs as the slip reaches the ground surface. One of the questions we will address in our analyses of four field examples is how close the tip of the slipped patch on the fault is to the ground surface at the time the deformation zone begins to form. We will see that the distance is expected to be on the order of the width of the deformation zone.

3. A Mechanical Model

[13] We will analyze deformation associated with a fault consisting of numerous dislocations that slip progressively from the lowest dislocation to the uppermost one (Figure 2), mainly based on the knowledge that earthquakes more often nucleate at depth [e.g., *Scholz*, 2002] and partly on the three general ideas we have described above but also on a set of simplifying assumptions that maintain the essential physics of the problems we want to address. Among the assumptions, the rheology of modeled material is elastic-plastic (Figure 3). We approximately model the strains at the ground surface by elastic strains computed with the solution for uniform slip with one or more dislocations. In particular, we describe the incremental permanent deformation associated with slipping dislocations by calculating the incremental elastic strains for a dislocation and then approximately calculating the incremental permanent strains with the elastic-plastic model for yielding, whose condition corresponds to a critical value of the deviatoric strain, $(\mathrm{II}_{\varepsilon'}^{e})_c$:

$$\mathrm{II}_{\varepsilon'}^{e} = \left(\frac{1}{2}\right)\varepsilon_{ij}^{\prime e}\varepsilon_{ij}^{\prime e}$$

$$\varepsilon_{ij}' = \varepsilon_{ij} - \varepsilon\delta_{ij}$$

$$\varepsilon = \left(\frac{1}{3}\right)\varepsilon_{kk}$$

where ε_{ij} is strain tensor, δ is Kronecker delta and the superscript of e means elastic.

[14] We simulate propagation of slip on a fault as shown in Figure 2. The fault exists before the simulated slip event occurs. It has a width of W_f and an infinite length. At time t_0 there is no slip on the fault and no strain in the medium. At time t_1, part of the fault of width δd_1 slips as an incremental dislocation as shown in Figure 2b. We model the deformation at each point along the ground surface caused by the mode II or mode III dislocation of width $W_d = \delta d_1$. At time t_2, the same amount of slip occurs on an adjacent part of the fault represented by another dislocation of width δd_2. Thus the tip of the slipped patch has propagated from the upper end of dislocation δd_1 to the upper end of dislocation δd_2. The tip of the slipped patch is now at $W_d = \delta d_1 + \delta d_2$ (Figure 2c). We model the additional deformation due to the additional dislocation at each point at the ground surface. This process is repeated in the simulation until the propagation is terminated or the slip breaks through the ground surface. The analysis of the problem is presented in Text S1 in the auxiliary material.[1]

4. Simulation of Strain Patterns and Zones of Permanent Deformation

4.1. Dip-Slip and Strike-Slip Faults

[15] The characteristics of theoretical zones of permanent surface deformation, which we identify with deformation zones observed in the field, are determined by the dip angle of the fault as well as whether the fault accommodates dip slip or strike slip and horizontal shortening or extension. Figure 4 compares zones of permanent surface deformation formed over a low-angle fault dipping 30° and slipping in either a right-lateral strike-slip sense (Figure 4, left) or a reverse dip-slip (Figure 4, right) sense. The boundary conditions at the ground surface are the same so that Figure 4 shows ways in which deformation is different for the two kinds of fault. Figures 4a–4d (left) show the plan view above and the cross section below at a stage of slip propagation. Slip begins at great depth for both types of fault and the tip of the slipped patch approaches the ground surface as dislocation patches of slip are added to the width, W_d, of the dislocation. As the width of the dislocation, W_d, approaches the width, W_f, of the fault, stresses and elastic strains at the ground surface become large enough to cause

[1] Auxiliary materials are available in the HTML. doi:10.1029/2009JB006361.

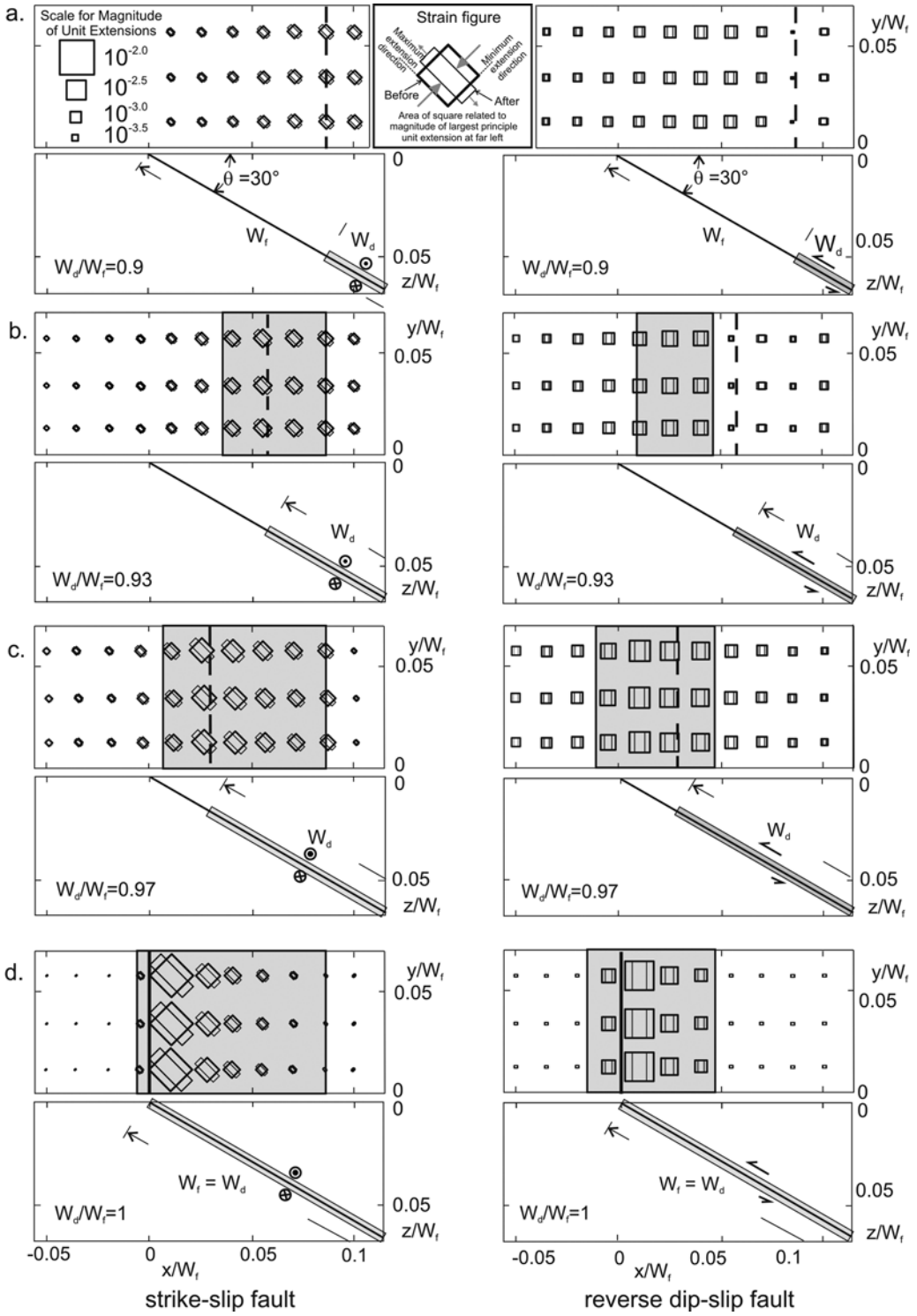

Figure 4. Development of zones of permanent deformation at ground surface over low-angle, 30° dip, strike-slip fault, and dip-slip fault at (a) $W_d/W_f = 0.9$; (b) $W_d/W_f = 0.93$; (c) $W_d/W_f = 0.97$; (d). $W_d/W_f = 1$, where W_d is the width of the dislocation and W_f is the width of the fault. The critical value of the second invariant of the deviatoric strain $(II^e_{\varepsilon'})_c = 10^{-6}$. The depth to the lower end of the fault is $D_f = W_f/2$. The fault slip, S, is 3×10^{-4} W_f. If W_f were 5 km, the depth to where the slip started would be at the depth $D_f = 2500$ m, and the fault slip would be $S = 1.5$ m. (left) Right-lateral, strike-slip fault. (right) Reverse, dip-slip fault.

permanent deformation. The zone of permanent deformation, shown with a gray rectangular area in plan view, widens as the slipped patch approaches and ultimately reaches the ground surface.

[16] The plan views in Figure 4 show a map of strains at each stage of slip propagation. The strains are shown with rectangular strain figures, which consist of a square and a rectangle. The area of the square indicates the magnitude of strain and the shape of the rectangle intimates the principal strains that transformed the square into the rectangle. The magnitude of the strain is read by comparing the square of a strain figure to a series of scaled squares such as those in the upper left of Figure 4a (left). Text S2 in the auxiliary material explains how to read the strain figures quantitatively.

[17] We start with a strike-slip fault. Figure 4 (left) shows four stages in the formation of a zone of permanent deformation at the ground surface caused by upward propagation of slip on a strike-slip fault (mode III propagation). We would note that only in stage 4 has the slip broken through the ground surface. In stages 1 through 3 the fault is "blind." Because the pattern of ground deformation evolves as the slip propagates, one can in principle use the deformation pattern to approximately characterize the faulting. Figure 4 (right) is for a reverse fault (mode II propagation) and the ratio of the width of the slipped part of the fault to the total length of the fault, W_d/W_f, for each stage is the same with its counterpart in Figure 4 (left). Two parameters for these two models are fixed: the dip angle, $\theta = 30°$, of the fault and the critical value of the second invariant of the deviatoric strain $(II^e_{\varepsilon'})_c = 10^{-6}$.

[18] Besides the strains, the main variables that change as the slip propagates are as follows:

[19] 1. D_{ts}/S is the depth ratio, where D_{ts} is the depth to the tip of the slipped patch on the fault and S is the slip. The value of particular interest is the depth ratio at which the zone of permanent deformation begins to form at the ground surface.

[20] 2. The term w/S is the normalized width of the zone of permanent deformation, where w is the width of the zone. The value we record is the normalized width when the slip has propagated to the ground surface.

[21] 3. The term w_b/w_f is the width ratio of the zone of permanent deformation behind, w_b, to that in front, w_f, of the projection of the tip of the slipped patch of a blind fault to the ground surface. This variable is of particular interest for blind faults.

[22] 4. The term w_{HW}/w_{FW}, the width ratio of the width, w_{HW}, of the zone of permanent deformation in the hanging wall to that in the footwall, w_{FW}. This ratio is the special case of w_b/w_f, where slip has propagated to the ground surface.

[23] At stage 1, the fault is blind (Figure 4a, left), and $W_d/W_f = 0.9$. The direction of maximum extensile strain, ε_1, is NW-SE if north is upward in the diagram. There is right-lateral, simple shear parallel to the trace of the fault. The largest deviatoric strain is approximately 10^{-3} so the second invariant of the elastic strains, $II^e_{\varepsilon'}$, is locally approximately 10^{-6}, that is, roughly equal to the critical value we have adopted for this problem. Two characteristics are: the deformation at the ground surface is right-lateral (same sense as fault) simple shear everywhere in the view. The strains are entirely elastic. The largest shear strain is approximately at the vertical projection of the tip of the slipped patch to the ground surface (dashed line in map view). At stage 2, $W_d/W_f = 0.93$. The zone of permanent deformation at the ground surface (gray) has initiated and widened within the hanging wall of the fault, and $w_b/w_f \cong 1.3$. The maximum strain (elastic and plastic) within the zone of permanent deformation remains essentially over the tip of the slipped patch. The largest shear strain remains approximately at the vertical projection of the tip of the slipped patch to the ground surface. At stage 3, $W_d/W_f = 0.97$, the zone of permanent deformation (gray) has widened. The ratio of w_b/w_f is $\sim$2.5. The largest shear strain remains approximately at the vertical projection of the tip of the slipped patch. At stage 4, the tip of the slipped patch has propagated to the ground surface so the zone of permanent deformation is complete; $W_d/W_f = 1$. The zone is highly asymmetric. It is quite narrow in the footwall and wide in the hanging wall of the fault so the plastic zone is almost entirely within the hanging wall; $w_{HW}/w_{FW} \cong 14$. The maximum permanent strain is, in principle, at the surface rupture.

[24] The idealized deformation zone for a low-angle, reverse fault develops rather differently than that for the low-angle, strike-slip fault. At stage 1, the strains normal to the surface trace of the fault change sign across the vertical projection of the tip of the slipped patch to the ground surface. At the vertical projection the strain is essentially zero; for the strike-slip fault it is maximal there. The deformation at the ground surface is shortening (same sense as fault) normal to the fault trace in front of the projection of the tip of the slipped patch to the ground surface. It is extension behind the projection. At stage 2, the zone of permanent deformation has initiated and widened. The permanent deformation appears well in front of the tip of the slipped patch. Indeed, the strains still change from horizontal shortening in front to extension behind the projection of the tip of the slipped patch. At stage 3, the zone of permanent deformation occurs mostly in front of the upward projection of the tip of the slipped patch for the reverse fault, whereas it was essentially over the tip of the slipped patch for the strike-slip fault. The zone of permanent deformation is mostly in front of the tip of the slipped patch and $w_b/w_f \cong 0.5$, but within the hanging wall of the fault, and $w_{HW}/w_{FW} \cong 4$. As the slip ruptures to the ground surface, at stage 4, the zone of permanent deformation is highly asymmetric with respect with the fault trace, and $w_{HW}/w_{FW} \cong 3$. The zone is quite narrow in the footwall and wide in the hanging wall of the fault for both for the strike-slip fault and the reverse-slip fault.

[25] The simulations shown in Figure 4 illustrate how mode III propagation of slip on a strike-slip fault and mode II propagation on a reverse fault from depth to the ground surface could produce somewhat different ratios, w_{HW}/w_{FW}, of widths of deformation zones in hanging walls and footwalls and highly different strain patterns. The strain pattern is a qualitative variable. The simulations suggest that if one could know where the termination of tip of the slipped patch of a blind fault projects to the ground surface and the strain pattern at the ground surface, one could determine the kind of blind fault. In all cases, though, the strain pattern should be diagnostic of the type of faulting.

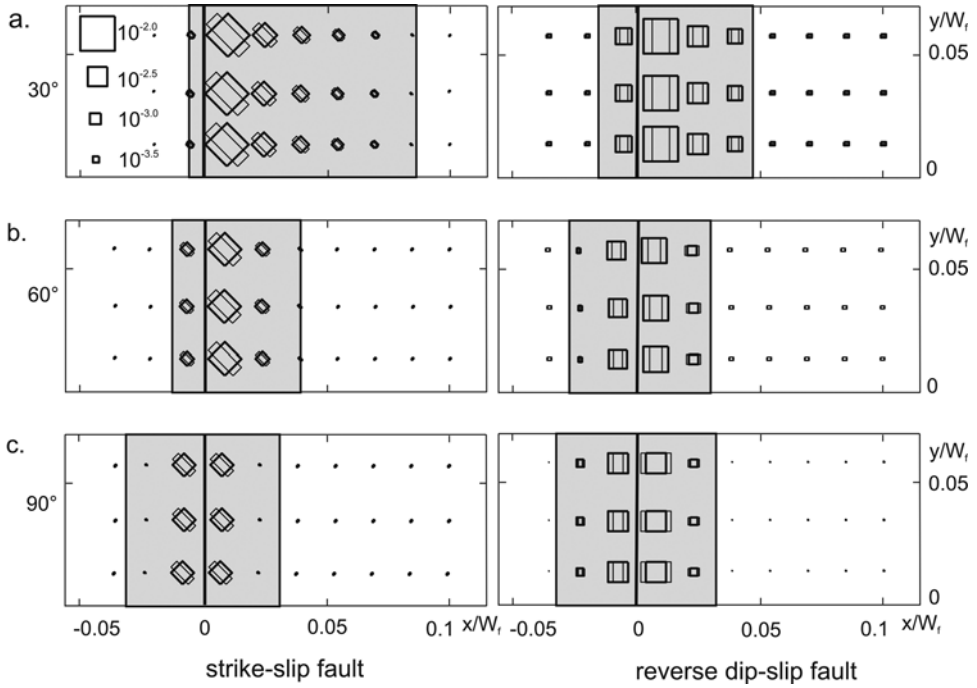

Figure 5. Idealized zones of permanent deformation for strike-slip and reverse-slip faults dipping at different angles. Faults in Figures 5a–5c dip to the right in the views. Slip has propagated to the ground surface; W_f is the width of the fault. (left) Right-lateral, strike-slip fault. All strains within the zones of permanent deformation display right-lateral sense like the sense of slip on the fault whereas strains outside of the zones display left-lateral sense. (a) Fault dip 30°; $w_{HW}/w_{FW} \cong 15$, where w_{HW} and w_{FW} are the widths of the zone of permanent deformation in the hanging wall and in the footwall, respectively. (b) Dip angle 60°; $w_{HW}/w_{FW} \cong 3$. (c) Dip of fault 90°; $w_{HW}/w_{FW} = 1$. (right) Reverse, dip-slip fault. In Figure 5a, fault dip 30°; $w_{HW}/w_{FW} \cong 3$, in Figure 5b, dip angle 60°; $w_{HW}/w_{FW} \cong 1.1$. Strains next to fault in hanging wall and in footwall are shortening. Away from fault trace the strains are shortening in footwall and extension in hanging wall. In Figure 5c, dip of fault 90°; $w_{HW}/w_{FW} = 1$. Strains are extension in direction normal to fault trace in uplifted block; strains are shortening in same direction in downthrown block.

4.2. Effect of Dip Angle

[26] The two examples in Figure 4 have shown how the idealized strain patterns, elastic and permanent, as well as characteristic variables, w/S and w_{HW}/w_{FW}, should ideally evolve as a function of slip propagation, W_d/W_f upward along the fault. Now we examine the characteristic variables, w/S and w_{HW}/w_{FW}, for strike-slip and dip-slip faults after the slip has propagated to the ground surface, for faults with three dip angles of $\theta = 30°$, 60° or 90° (Figure 5).

[27] We have already seen for the faults dipping 30° beneath the hanging wall: for both types of fault, the position of the fault trace is much closer to one side of the zone of permanent deformation than the other (Figure 5a). The fault dips beneath the widest part of the deformation zone. A corollary is that the width of the zone of permanent deformation is significantly wider in the hanging wall block than in the footwall block for both kinds of faults; $w_{HW}/w_{FW} > 1$.

[28] For the vertical faults (Figure 5c), we see two strong features: the *pattern of strains* in the zone of permanent deformation is diagnostic. It is symmetric across the strike-slip fault and antisymmetric across the dip-slip fault (Figure 5c). The *position of the fault trace* is at midwidth of the zone of permanent deformation for both vertical strike-slip and dip-slip faults.

[29] The results for the faults dipping 60° are unsurprising in the context of Figure 5 because they are intermediate between those for faults dipping 30° or 90°. There are, however, distinctive differences between dip-slip and strike-slip zones of permanent deformation if the dip is 60°: the position of the fault trace, that is, w_{HW}/w_{FW}, for the $\theta = 60°$ dip-slip fault is more nearly like that of the vertical dip-slip fault, $\theta = 90°$. The position of the fault trace for the $\theta = 60°$ strike-slip fault is more nearly like that of the $\theta = 30°$ strike-slip fault. It follows that the width of the zone of permanent deformation is significantly narrower in the footwall block than in the hanging wall block for $\theta = 60°$ strike-slip faults; $w_{HW}/w_{FW} > 1$. The widths of deformation zones are more nearly equal, $w_{HW}/w_{FW} \cong 1$, in the two blocks for $\theta = 60°$ dip-slip faults. For both of the 60° faults, however, the strains are significantly larger in the hanging wall than in the footwall.

4.3. Normal and Reverse Dip-slip Faults

[30] Figure 6 compares the strain patterns for normal and reverse dip-slip faults, the slip on which has extended to the ground surface. The only possible difference in the idealized deformation zones is a matter of symmetry; nevertheless, it might be helpful to see the difference: for a normal fault the strain with the largest magnitude is extension whereas for a reverse fault the strain with the largest magnitude is short-

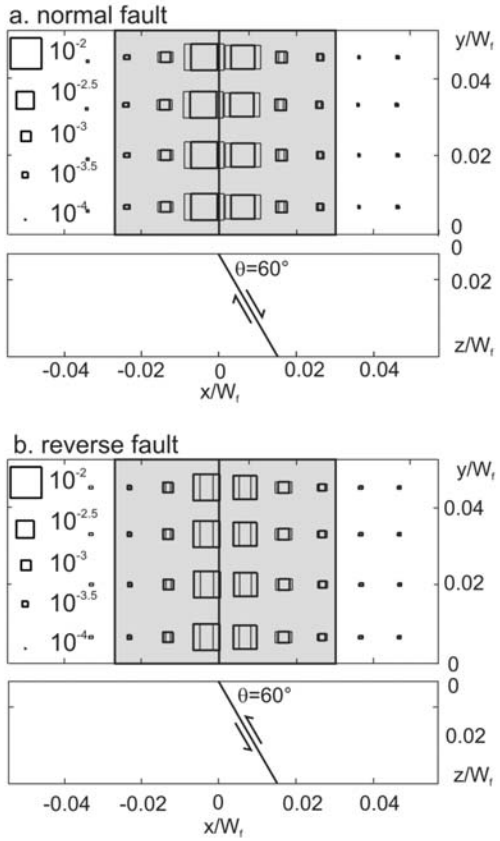

Figure 6. Final zone of permanent deformation for a dip-slip, normal fault dipping at 60° and a dip-slip, reverse fault dipping at the same angle. (a) The normal fault. Strains next to fault in hanging wall and in footwall are extension. Away from fault trace the strains are extension in footwall and shortening in hanging wall. (b) The reverse fault. Strains next to fault in hanging wall and in footwall are shortening. Away from fault trace the strains are shortening in footwall and extension in hanging wall.

ening. For both types of fault, the wider zone of permanent deformation is in the hanging wall block. The slip direction of the blind fault is determined by the ratio, w_S/w_E, where w_S is the width of the shortening belt and w_E is the width of the extension belt. If the ratio is <1, the fault is a normal fault. If the ratio is >1, the fault is a reverse fault.

[31] We note that although the larger strain is extension for the normal fault and shortening for the reverse fault, the only type of failure possible in the elastic-plastic theory is plastic yielding, so the theory cannot be expected to recognize that failure in horizontal tension is generally quite different from failure in horizontal compression in earth materials. Finally, an observation that is relevant to the interpretation of the type of blind fault at Winnetka that we describe in following paragraphs: the strain with the largest magnitude is a shortening for the reverse fault (Figures 4, right, 5, right, and 6b) and an extension for the normal fault (Figure 6a).

[32] These are the general characteristics for strike-slip and dip-slip faults according to the theoretical model that we use to understand some features of deformation zones.

5. Some Estimates of the Critical Deviatoric Strain Invariant

[33] It is helpful to have some idea about the range of values that one might expect for the parameter we call the critical deviatoric strain invariant for plastic yielding, $(II^e_{\varepsilon'})_c$. In doing so, we liberally interpret what the parameter might represent. Table 1 shows low and high estimates of representative deviatoric strain, ${}_r\varepsilon'_c$, and corresponding critical second invariant, $(II^e_{\varepsilon'})_c$, where

$$ {}_r\varepsilon'_c = \pm\sqrt{\left(\mathrm{II}^e_{\varepsilon'}\right)_c} $$

for measurements that we have made in the field and in the laboratory. Some estimates of representative deviatoric strain, ${}_r\varepsilon'_c$, and critical second invariant, $(II^e_{\varepsilon'})_c$, are given in Table 1.

[34] The brittle materials include cylindrical specimens of granite, and concrete in sidewalks, curbs and foundations. The more ductile materials include soil, landslide debris (loaded in the field in horizontal tension and compression) and asphalt pavement. For example, ground strains measured in an area of extensively fractured ground, pavement and sidewalks in the Granada Hills area, Los Angeles, California, that was damaged during the Northridge earthquake, were typically 3×10^{-3}, but maximum strains ranged up to 10^{-2} [*Johnson et al.*, 1996a]. In the Winnetka area of the Northridge earthquake [*Cruikshank et al.*, 1996], the ground strains were much smaller, on the order of 3×10^{-4}, than in the Granada Hills area. Perhaps the strains in much of the Winnetka area, where there was minimal cracking and damage to utilities, were mainly elastic. This might explain

Table 1. Estimates of Critical Invariant of Deviatoric Strain Parameter $(II^e_{\varepsilon'})_c$

Material	Critical Value (Low)			Critical Value (High)		
	Representative Strain ${}_r\varepsilon'^{\,a}_c$	Invariant $(II^e_{\varepsilon'})_c$	Exponent n (10^n)	Representative Strain ${}_r\varepsilon'_c$	Invariant $(II^e_{\varepsilon'})_c$	Exponent n (10^n)
Granite (shortening)[b]	-2×10^{-3}	4×10^{-6}	−5.4	-0.6×10^{-2}	4×10^{-5}	−4.4
Landslide debris (shortening)[c]	-14×10^{-3}	2×10^{-4}	−3.7	-2×10^{-2}	4×10^{-4}	−3.4
Landslide debris (extension)[c]	6×10^{-3}	4×10^{-5}	−4.4	3×10^{-2}	10^{-3}	−3
Concrete, asphalt, soil (extension)[d]	3×10^{-3}	10^{-5}	−5	10^{-2}	10^{-4}	−4
Concrete, asphalt, soil (extension)[e]	0.3×10^{-3}	10^{-7}	−7	0.1×10^{-2}	10^{-6}	−6

[a]Note that the relative critical strain ${}_r\varepsilon'_c$ is the square root of $(II^e_{\varepsilon'})_c$; n is the $\log_{10}$ of $(II^e_{\varepsilon'})_c$.
[b]Chelmsford granite. From *Peng and Johnson* [1972].
[c]Aspen Grove landslide debris. From *Fleming and Johnson* [1989] and *Baum et al.* [1988, 1993].
[d]Granada Hills, 1994. From *Johnson et al.* [1996a].
[e]Winnetka, 1994. From *Cruikshank et al.* [1996].

the very small values in the concrete, asphalt, soil (extension) for Winnetka 1994 in Table 1. Where strains were somewhat larger, up to 10^{-3}, there was modest cracking and damage at Winnetka, but the types of damaged mapped mainly reflected extension. The estimates for landslide debris are based on measurements of strains prior to failure in landslide debris at Aspen Grove, Utah [*Fleming and Johnson*, 1989].

6. Graphical Determination of Characteristic Parameters

[35] We have compiled three diagrams in order to help one estimate a couple of parameters for a deformation zone. The diagrams are in terms of dimensionless parameters. We have selected the amount of slip, S, to normalize many lengths because it commonly can be estimated. The dimensionless parameters used in the theoretical analyses are the ratio of the fault width to the slip, W_f/S, the dip angle of the fault, θ (degrees), and the critical invariant of the deviatoric elastic strain, $(II^e_{\varepsilon'})_c$. Other dimensionless variables that we can determine with numerical solutions are the ratio of the width of the deformation zone in the hanging wall to that in the footwall, w_{HW}/w_{FW}, and the ratio of the total width of $w = w_{HW} + w_{FW}$, of the deformation zone to the slip, w/S. These dimensionless variables are interrelated in Figure 7.

[36] The width ratio, w_{HW}/w_{FW}, of the deformation zone is particularly useful because it relates well to the dip angle, θ, of the fault. The two curves in Figure 7a show the width ratio, w_{HW}/w_{FW}, as a function of dip angle, θ, for strike-slip and dip-slip faults. The curves were calculated for a wide range of critical invariants, $(II^e_{\varepsilon'})_c$, but the curves were indistinguishable, so only two curves need to be plotted. Thus, if one knows dip angle, θ, one can estimate the width ratio, w_{HW}/w_{FW}. Or if one knows the width ratio, one can estimate the dip angle.

[37] The relations between the total width of the deformation zone and the critical invariant of deviatoric strain depend on the dip angle, so Figures 7b and 7c show the relations for strike-slip and dip-slip faults, respectively. The total width is represented in its dimensionless form, w/S, and the critical invariant of the deviatoric elastic strain, $(II^e_{\varepsilon'})_c$, is represented by its exponential form, n, where $(II^e_{\varepsilon'})_c = 10^n$. Thus, one first uses the appropriate curve in Figure 7a to determine the dip angle of the fault from measurement of the width ratio, w_{HW}/w_{FW}, and then one uses the curves in either Figure 7b for strike-slip faults or Figure 7c for dip-slip faults to determine either w/S or $(II^e_{\varepsilon'})_c$, depending which is unknown.

[38] The results shown in Figure 7 were calculated for a W_f/S ratio of 3333. For very wide faults, say $W_f/w > 500$ or 1000, the results should be insensitive to the total width of the fault because the zone of permanent deformation does not appear until the tip of the slipped patch is rather near the ground surface, as suggested by the results in Figure 4.

7. Analysis of Deformation Belts Along Some Earthquake Ruptures

7.1. Right-Lateral Deformation Zone Beneath Kaynaşlı Viaduct, Turkey

[39] The fault trace of the 12 November 1999 earthquake in the Düzce-Bolu region in Anatolia crossed the 2.4 km long alignment of a new viaduct at Kaynaşlı, Turkey. Surveys of the piers provided a very rare record of ground deformation along an earthquake rupture because the piers had been surveyed before and after the earthquake. In effect, each group of four piers that supported the viaduct was a giant strain gauge that spanned the earthquake rupture zone and yielded data about ground movement and distortion near the fault.

[40] The surveys show that along the right-lateral rupture at Kaynaşlı the fault zone consists of a belt of large, right-lateral distortion containing the main trace with right-lateral offset and is bounded by small, left-lateral distortion on the north. The data and the results of strain and displacement analyses are presented elsewhere [*Johnson et al.*, 2002; *Gür*, 2004]. At the intersection of the Kaynaşlı Viaduct and the main rupture, the rupture crossed a service road at an acute angle with the south edge of the viaduct and trended eastward toward pier R45, under the eastbound lane of the viaduct (supported by piers R, Figure 8a). The main rupture was perhaps a meter wide and the offset across the main rupture was 1.15 m, right-lateral (A. Barka and E. Altunel, Preliminary report on whether the Asursu Valley is active fault controlled, unpublished consulting report to ASTALDI-BAYINDIR Co., 28 pp., 2000). Measurements of piers along the entire viaduct indicate 2.1 m of offset across the deformation zone [*Gür*, 2004], so ~55% of the offset occurred along the main rupture. The rest was distributed through the deformation zone and is presumably reflected in the strain measurements.

[41] Deformation computed from surveys of horizontal positions of piers before and after the earthquake [*Johnson et al.*, 2002] show that the maximum shear strain $|(\varepsilon_1 - \varepsilon_2)/2|$ is largest near where the main rupture passed beneath the viaduct, but the strains are significant for about 450 m of the length of the viaduct involving all the piers between piers 39 and 49 (Figure 8b). Quadrilaterals involving piers 45 to 48 have the highest shear strains, ranging from 1.5×10^{-2} to 5×10^{-2}. Quadrilaterals involving piers 38 to 44 in the western part of the deformation zone have smaller maximum shear strains, approximately 10^{-2}. The azimuths of the maximum extension directions for the quadrilaterals complete the picture of the strain of ground beneath the viaduct (Figure 8b). They indicate a right-lateral deformation zone with boundaries roughly parallel to the trend of the main rupture.

[42] The central question for our analysis of the Kaynaşlı deformation zone is whether one can fit the results of the slip propagation theory to the salient field observations and measurements. *Bürgmann et al.* [2002] have suggested that the Düzce fault dips approximately 54° north according to inversion of displacements of global positioning system (GPS) sites together with interferometric synthetic aperture radar range change data through a model of rectangular dislocations in an elastic, homogenous, and isotropic half-space. The dimensional parameters of the part of the fault that slipped were approximately: length of 40 km and width of $W_f = 20$ km [*Umutlu et al.*, 2004]. We assume that the length is essentially infinite in the analysis. The slip at depth on the fault in the Kaynaşlı area was approximately $S = 3$ m [*Akyüz et al.*, 2002]. The characteristic parameters according to the theory are summarized in Table 2.

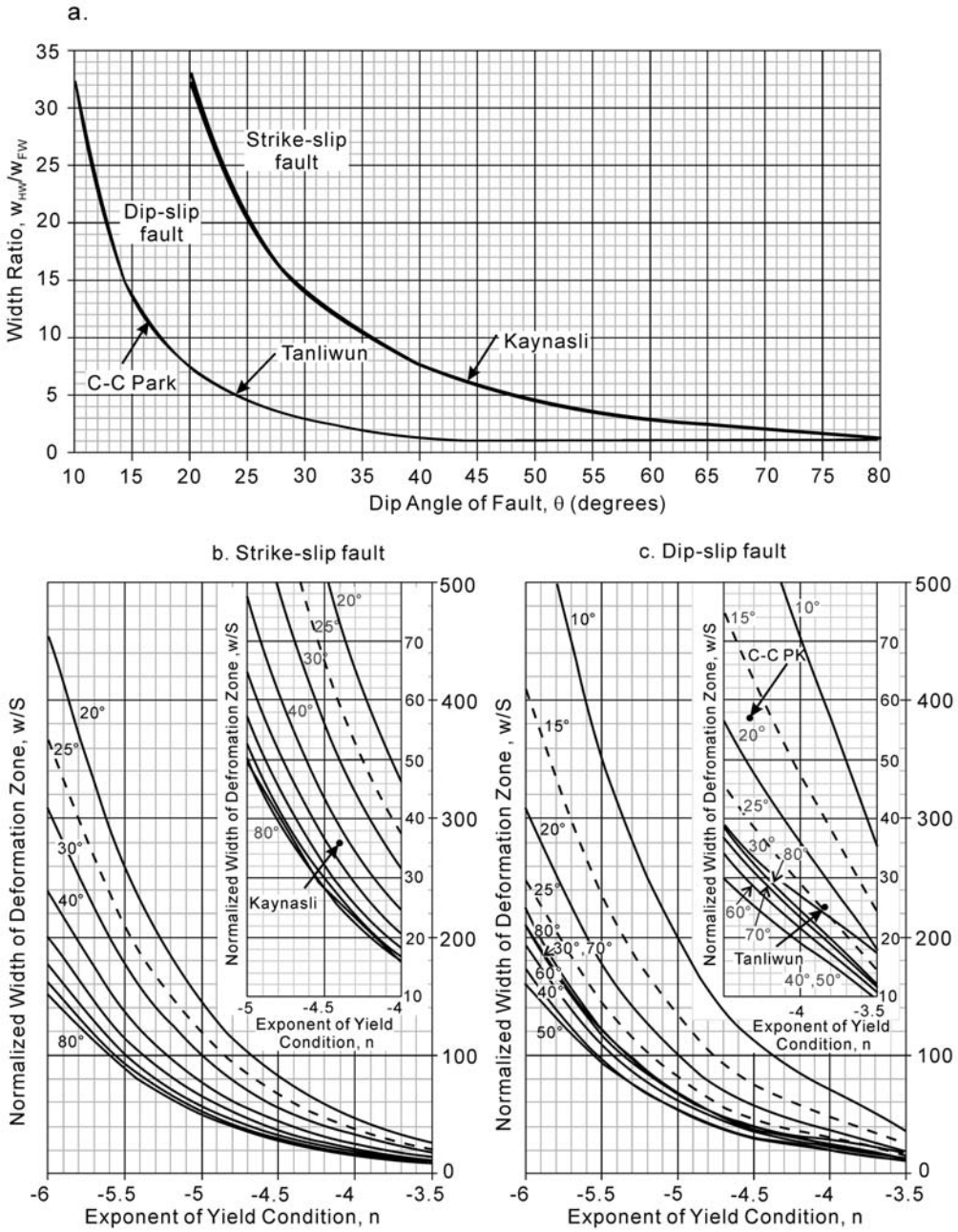

Figure 7. Relations among variables for zones of permanent deformation. The normalized width of the fault is constant, $W_f/S = 3333$. C-C Park is Chung-Cheng Park. The curves show that the width ratio, w_{HW}/w_{FW}, is sensitive to the fault type, the dip angle, θ, and the critical second invariant, $(II^e_{\varepsilon'})_c$. (a) Width ratio as a function of fault dip, θ, and fault type. The relations have been plotted for a wide range of values of $(II^e_{\varepsilon'})_c$, the critical second invariant of deviatoric strains, but the plots superpose nearly perfectly so the relations are apparently independent of the critical second invariant. (b) Strike-slip fault. The ratio of the total width of the deformation zone to the fault slip, w/S, as a function of the fault dip angle, θ, and the exponent, n, of the critical second invariant. Each curve represents a different dip angle. (c) Dip-slip fault. Relations are among the same variables.

[43] The salient features are that the deformation zone at Kaynaşlı was approximately $w = 110$ m wide. The main rupture, the Düzce fault at Kaynaşlı, was near the south side of the deformation zone. The ratio of the width of the deformation zone in the hanging wall to that in the footwall of the main rupture was approximately $w_{HW}/w_{FW} = 6$. The amount of offset across the deformation zone at the ground surface was 2.1 m at Kaynaşlı viaduct (Table 2).

[44] In order to derive a solution with the theoretical model we assume that we know the fault width, W_f, and the amount of slip, S (Table 2, measured value) and do not vary these parameters. We vary dip angle, θ, and yield condition, $(II^e_{\varepsilon'})_c$. We have an estimate of the dip angle for the entire

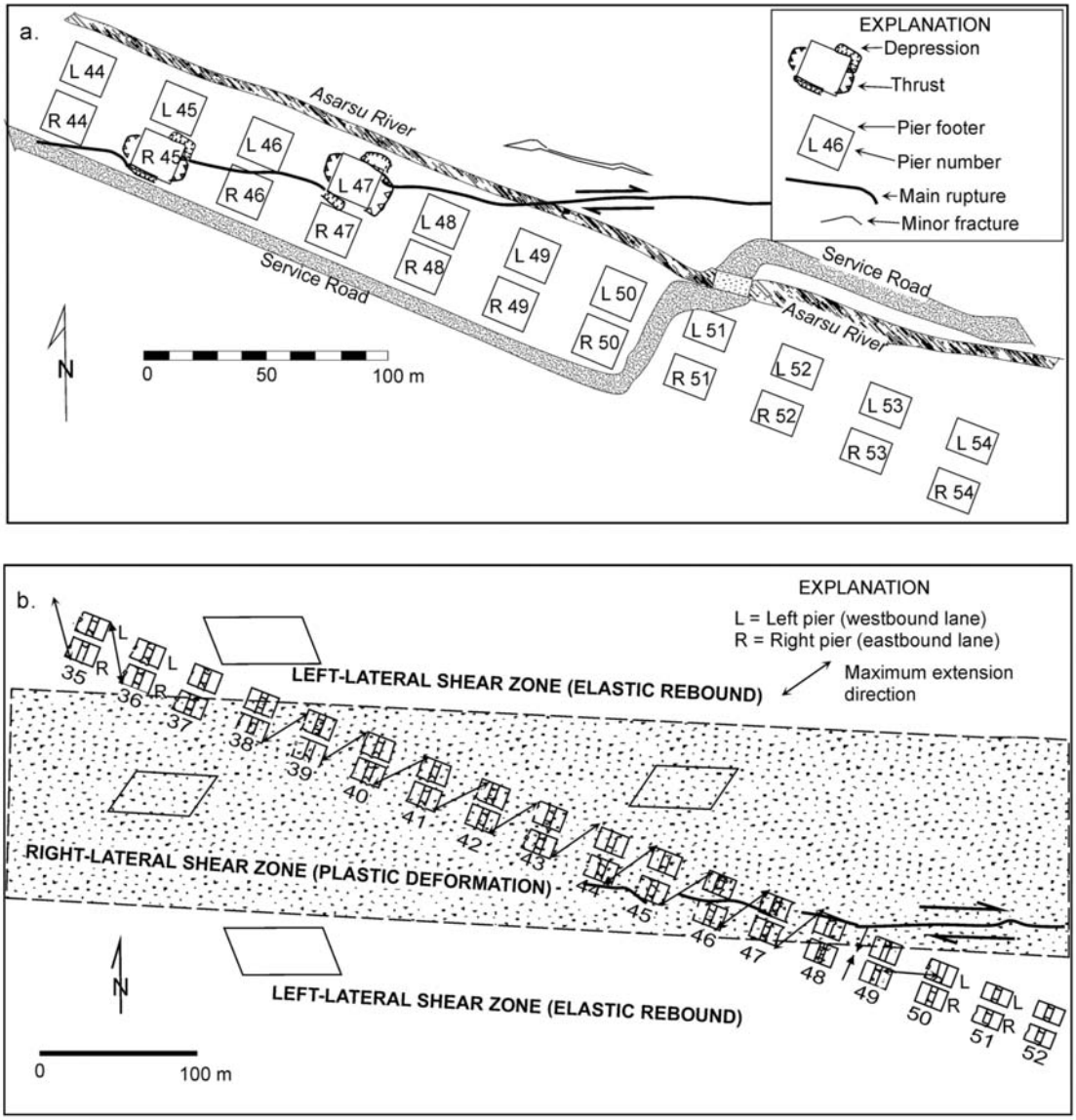

Figure 8. Deformation zone beneath Kaynaşlı Viaduct, Turkey (modified by *Johnson et al.* [2002] (with kind permission of Springer Science and Business Media) after ASTALDI-BAYINDIR Co.). (a) Trace of main rupture beneath Kaynaşlı Viaduct. Rectangles represent pier caps. The viaduct intersects the earthquake rupture at an angle of approximately 15°. (b) The Kaynaşlı right-lateral deformation zone. The double-headed arrows show azimuths of maximum extension along the viaduct. Orientations indicate right-lateral shearing between piers 38 and 48 and left-lateral shearing between piers 34 and 36. Strains were too small to analyze south of the deformation zone so the left-lateral shearing indicated there is hypothetical.

Düzce-Bolu fault but we use that estimate to check the result determined with the theory. The yield condition is an empirical parameter. Thus, all we can do with the yield value is to compare the calculated values with the field and laboratory estimates of critical values of deviatoric strain reported in Table 1.

[45] As shown for the deformation zone at the Kaynaşlı viaduct in Table 3, based on the known value of the parameter, $w_{HW}/w_{FW} = 6$, we can use Figure 7a to compute the dip angle, θ, of the fault: $\theta = 44°$. Furthermore, we can use the dip angle, θ, and the normalized width of the deformation zone, $w/S = 36$, to estimate n, the exponent of the yield condition, $n = -4.4$ (Figure 7b). The exponent can also be expressed in terms of the critical invariant of the deviatoric strains, that is, the yield criterion, $(II^e_{\varepsilon'})_c = 0.4 \times 10^{-4}$ or in terms of the representative critical strain, ${}_r\varepsilon'_c = 6.3 \times 10^{-3}$. The value determined for the critical invariant, $(II^e_{\varepsilon'})_c$ is comparable to the high end of values for Chelmsford Granite and the low end of values for landslide debris (Table 1).

[46] Some information about the beginning of formation of the deformation zone, which is not determined by the graphical solutions in Figure 7, is derived from a numerical simulation for this model. It is natural to wonder how close

Table 2. Values of Parameters for Kaynaşlı Deformation Zone

Parameter	Measured	Assumed	Varied	Calculated
Fault width, W_f (m)		Yes, 20000[a]		
Width deformation zone, w (m)	110[b]			108
Slip, S (m)	2.1[b]	Yes, 3[c]		
Width ratio, w_{HW}/w_{FW}	6[b]			
Dip of fault, θ (deg)	54 N[d]		Yes	44 N
Normalized width deformation zone, w/S	36.7			36
Exponent of yield condition, n[e] (10^n)			Yes	−4.4

[a] *Umutlu et al.* [2004].
[b] *Johnson et al.* [2002] and *Gür* [2004].
[c] *Akyüz et al.* [2002].
[d] *Bürgmann et al.* [2002].
[e] Note that $10^n = (II^e_{\varepsilon'})_c$.

the tip of the slipped fault is to the ground surface when the deformation zone begins to form. We have no observations, but the theory suggests an answer to the question. The tip of the slipped patch of the strike-slip fault at Kaynaşlı was approximately 74 m deep when the deformation zone began to form (Table 4). The width of the deformation zone ultimately was approximately 110 m, so the tip was quite shallow. The tip of the slipped patch was approximately 76 m north of the trace of the ultimate surface rupture at Kaynaşlı (Table 4) as the deformation zone started to form.

[47] The value calculated for the dip angle of the fault near the southern end of the Düzce fault at Kaynasli is θ = 44° N, which is 10° lower than the one calculated by *Bürgmann et al.* [2002] for the entire Düzce fault, but both solutions provide a north dipping, strike-slip fault. We have shown that the width ratio of w_{HW}/w_{FW} = 6, as determined from strain measurements (Figure 10), indicates a dip angle of 44°. If the fault angle were selected to be 54°, as determined by *Bürgmann et al.* [2002, Table 2], the calculated width ratio, w_{HW}/w_{FW} = 4, would have been much smaller than that measured. A 10° difference in dip angles determined by these two quite different methods, however, would not be surprising.

7.2. Thrust Deformation Zone at Chung-Cheng Park, Taiwan

[48] The ground rupture of the 1999 Chi-Chi earthquake in Taiwan caused much of the damage to dwellings, large structures and infrastructure of communities through which the rupture passed [*Taiwan Central Geological Survey* (*TCGS*), 1999a, 1999b; *Kelson et al.*, 2001; *Dong et al.*, 2004; NCREE, online database, 2000]. East of the city of Fengyuan, near the northern end of the Chi-Chi rupture, the deformation zone along the ground rupture was about 350 m wide at Chung-Cheng Park and in the hills to the south (Figure 9a). The Chung-Cheng Park deformation zone was defined by opposite facing escarpments and smaller, internal structures (Figure 9b). The ground appeared to be undeformed to the east and west of the deformation zone. The escarpment on the west side of the deformation zone was the leading edge of the Chi-Chi thrust fault, which formed along the mountain front. It was west facing and 4.5 to 5 m high. Along the leading edge of the Chi-Chi rupture belt at the west side of the park was a disrupted zone about 15 m wide of intense deformation extending from the base to the crest of the western escarpment. The most severe building damage was in that area (Figure 9a). All the buildings were partly damaged to completely destroyed; many were tilted. The damage was mostly caused by ground deformation and fracturing [*Huang*, 2006; NCREE, online database, 2000]. The escarpment on the eastern side of the deformation zone was east facing and up to 1.5 m high. It could be traced for about 250 m across the valley bottom. Its height diminished toward the south, so the escarpment may well have formed only in the alluvium in the valley bottom.

Table 4. Locations of Tip of the Slipped Patch when Permanent Ground Deformation Began for Three Deformation Zones

Parameter	Kaynaşlı	Chung-Cheng Park	Tanliwun
Fault type	strike slip	thrust	thrust
Dip angle, θ (deg)	44	16.5	24
Vertical distance from ground surface to tip of the slipped patch, D_{ts} (m)	74	122	44
Horizontal distance from tip of the slipped patch to ultimate surface rupture, w_t (m)	76	410	98

[49] The geologic structures within the Chung-Cheng Park deformation zone along Han River include small anticlines and synclines, low monoclinal escarpments, fractures, and cracks. These small structures occur throughout the width of the deformation belt (Figure 9b). The most common structure in the asphalt road in Han River Valley was open fractures, tension cracks, and some high-angle, reverse faults. There were several low-amplitude, anticlinal and synclinal folds in the asphalt road. The relief of the folds ranged from 0.15 m to 0.4 m [*Huang*, 2006]. *Dong et al.* [2004] examined damage to man-made structures in the residential development on the hilltop, south of Han River, and mapped a west facing, monoclinal escarpment with vertical uplift of 10 to 20 cm trending N12°E in that area (Figure 9a).

Table 3. Characteristic Parameters Estimated with Graphical Solutions for Three Deformation Zones

Parameter	Kaynaşlı	Chung-Cheng Park	Tanliwun
Ratio of width of hanging wall to footwall, w_{HW}/w_{FW} [a]	6	11.5	5
Dip angle of fault, θ[a] (deg)	44	16.5	24
Normalized width of deformation zone, w/S [b]	36	57	24 to 26
Exponent in value of yield condition, n[b] (10^n)	−4.4	−4.3	−3.8 to −3.9
Critical deviatoric strain invariant, $(II^e_{\varepsilon'})_c$[c]	0.4×10^{-4}	0.5×10^{-4}	1.41×10^{-4}
Relative critical strain, $_r\varepsilon'_c$	0.63×10^{-2}.	0.67×10^{-2}	1.1 to 1.3 $\times 10^{-2}$

[a] Values shown in Figure 7a.
[b] Values shown in Figure 7b or 7c.
[c] Note that $(II^e_{\varepsilon'})_c = 10^n$; $_r\varepsilon'_c = \sqrt{(II^e_{\varepsilon'})_c}$.

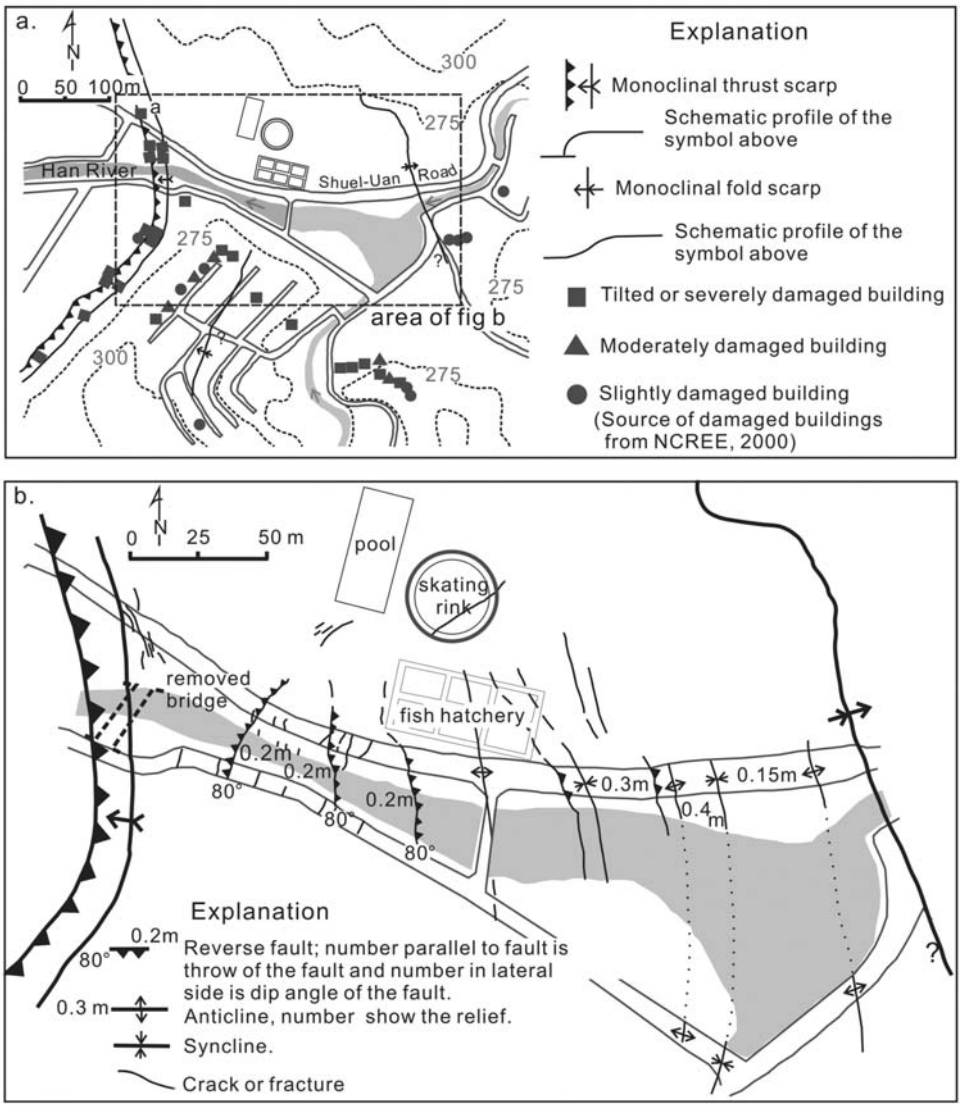

Figure 9. Deformation features in Chung-Cheng Park. The structures shown on the two maps are collated data by W.-J. Huang and data from maps (corrected by W.-J. Huang) by *Kelson et al.* [2001] and *Dong et al.* [2004]. (a) Escarpments on each side of deformation zone and distribution of building damage. Two opposite facing escarpments, a monoclinal thrust escarpment on the west and a monoclinal escarpment on the east bound the deformation zone. Square, triangle, or circle shows location of a damaged building (NCREE, online database, 2000). Buildings were damaged mostly within the deformation zone, but damage was especially high near the west facing escarpment. (b) Deformation features between the two opposite facing escarpments. The features include removed bridge, high-angle reverse faults, fractures, cracks, and low-amplitude folds.

[50] *Lee et al.* [2003] reported that the western escarpment accommodated oblique shift, 4.5 m of vertical slip and 6.4 m of strike slip, and 2.5 m of shortening. They inferred an underlying fault dipping approximately 60° east. We argue that their estimates of the fault angle and fault slip contain errors or reflect variations in near-surface conditions for the following reasons: (1) The lengths of their measurements at the ground surface are only few tens of meters. (2) Their estimate of fault slip relies on their subjective determination of fault strike based on the trend of the Chi-Chi fault trace at that site. (3) Our observations did not reveal left-lateral shift within the deformation zone. (4) The fault angle should be low (probably less than 30° based on the rule of V's) because the fault trace formed a V shape and followed the same contour at the valley on a map with a scale of 1:25000 [*TCGS*, 1999a, 1999b]. (5) A building straddling the large, western escarpment (building a in Figure 9a) was squeezed and lifted up but not torn laterally or visibly rotated.

[51] We have chosen to analyze the faulting beneath Chung-Cheng Park to be pure reverse faulting, the toe of a thrust sheet, in the theoretical model of the formation of the deformation zone. The small high-angle reverse faults, low-amplitude folds and fractures within the deformation zone (Figure 9b), indicate that the direction of maximum compression in the park was normal to the overall trend of

Table 5. Values of Parameters for Chung-Cheng Park Deformation Zone

Parameter	Measured	Assumed	Varied	Calculated
Fault width, W_f (m)		Yes, 30×10^3[a]		
Width of deformation zone, w (m)	350[b]			346
Slip, S[d] (m)	VS 4.5 to 5[b]; RDS 6[c]	Yes, 6		
Width ratio, w_{HW}/w_{FW}	11.5[b]			
Fault dip angle, θ (deg)	20 to 30 E[a]		Yes	16.5 E
Normalized width of deformation zone, w/S				57
Exponent in value of yield condition, n (10^n)			Yes	−4.3

[a] *Kao and Chen* [2000].
[b] *Huang* [2006].
[c] W. S. Chen (Investigation of earthquake geology and database construction of active faults (in Chinese), 2002, available at http://cgsweb.moeacgs.gov.tw/CGSWeb/result/Fault/web/chen%20wen-shan/reserch2_pic11pic12.htm). Note that the slip was estimated based on the offset across a shear zone at a trench about 200 m southwest of Chung-Cheng Park.
[d] VS is vertical slip; RDS is reverse, dip slip.

the Chi-Chi fault trace in the area. GPS data indicate that directions of horizontal components of displacement are normal to the trace of the Chi-Chi earthquake rupture at the park [*Yu et al.*, 2001]. Although the Chung-Cheng Park structure may well not have been a simple thrust toe, the much larger escarpment on the west side than on the east side suggests that we can approximately analyze the structure as a thrust toe.

[52] The geometric parameters for the fault of the Chi-Chi earthquake were determined by *Kao and Chen* [2000]: fault length 80 km; fault width W_f = 30 km; fault dip θ = 20° to 30° E. The deformation zone at Chung-Cheng Park was highly asymmetric: the width ratio of hanging wall to footwall was approximately w_{HW}/w_{FW} = 11.5. The total width of the deformation zone was about 350 m. Our best estimate of the dip slip on the fault on the west side of the zone is 6 m. The origins of the estimates of the parameters of the Chung-Cheng Park deformation zone are shown in Table 5.

[53] As indicated in Table 5, two parameters were adjusted in order to model the shear zone at Chung-Cheng Park: the exponential form of the critical yield condition, n, in 10^n, and the dip angle, θ, of the fault. Two parameters are fixed, the fault width, $W_f = 30 \times 10^3$ m and the amount of reverse slip, S = 6 m. Three other quantities were measured in the field and are therefore known: the width of the deformation zone in the hanging wall, w_{HW}, and footwall, w_{FW}, and the total width, w, of the deformation zone.

[54] Using the curve for a dip-slip fault in Figure 7a, the value of w_{HW}/w_{FW} = 11.5 corresponds to a dip angle of θ = 16.5°, as recorded in Table 3. Using that dip angle and the normalized width of the deformation zone, w/S = 57 in Figure 7c, we can estimate the exponent of the critical second invariant of the deviatoric strains to be approximately −4.3, so that $(II^e_{\varepsilon'})_c = 10^{-4.3} = 0.50 \times 10^{-4}$ (Table 3). It is comparable to the low values for Aspen Grove landslide debris and the materials in the Granada Hills area, as well as the alluvium beneath the Kaynaşlı Viaduct (Table 1). Comparing the calculated dip angle θ = 16.5° east to dips estimated by others (Table 5), we see that it is near the lower end of the range of dips, 20° to 30° east, determined by *Kao and Chen* [2000].

[55] The deformation zone began to form when the tip of the slipped patch was approximately 428 m down the dip of the fault. The solution suggests that the tip of the slipped patch was at that time 122 m deep vertically and 410 m east, horizontally, from where the rupture at Chi-Chi came to the ground surface (Table 4).

7.3. Thrust Deformation Zone at Tanliwun, Taiwan

[56] Parts of a deformation zone at Tanliwun, near Chushan, in the southern part of the Chi-Chi rupture, have been described by *Huang* [2006], who mapped some features of the deformation zone in detail. Approximate boundaries of the deformation zone are shown in Figure 10a. The average width of the deformation zone was w = 80 m. The escarpment at the leading edge of the thrust sheet was 1 to 2 m high. The trace of the escarpment rather closely followed the trace of the western edge of the foothills throughout the Tanliwun area (Figure 10a).

[57] A trench (location A, Figure 10a) dug across the escarpment of the main Chi-Chi rupture shows that the fault zone was 4 to 5 m broad and that about half the horizontal displacement of 3.4 to 4 m in 1999 was accommodated by the faults in Chushan trench. The ground deformation exposed within the trench is restricted to the immediate vicinity of the escarpment and its subsurface counterpart [*Huang*, 2006]. Differential horizontal displacements of approximately 1 to 2 m were accommodated by the rest of the deformation zone. There are few deformation features west of the escarpment in the footwall of the Chi-Chi rupture.

[58] Fractures in a Shanhu Yuan in the hanging wall of the Chi-Chi thrust (location B, Figure 10a) 60 m NE of the trench were mapped in detail in order to analyze the deformation in part of the hanging wall of the Tanliwun deformation zone (Figure 10b) [*Huang*, 2006]. All the features were a result of horizontal compression in the NE-SW direction as well as sufficient horizontal tension NW-SE to produce tension cracks. The direction of compression in the courtyard, then, was parallel to the direction of compression in the Chushan trench as indicated by the faulting and folding exposed in the trench. GPS data in the area also indicates that the direction of horizontal component of displacement is normal to the general trace of the Chi-Chi rupture at Tanliwun [*Yu et al.*, 2001].

[59] The example of a deformation zone at Tanliwun is unusual in that we know the dip angle, θ, of the fault but not the width ratio, w_{HW}/w_{FW}, of the deformation zone, so we use the dip angle to estimate the width ratio, for example, with Figure 7a. A fault dip angle of 24° was calculated for the Chushan trench site using surface and subsurface information, including a borehole drilled NE of the trench

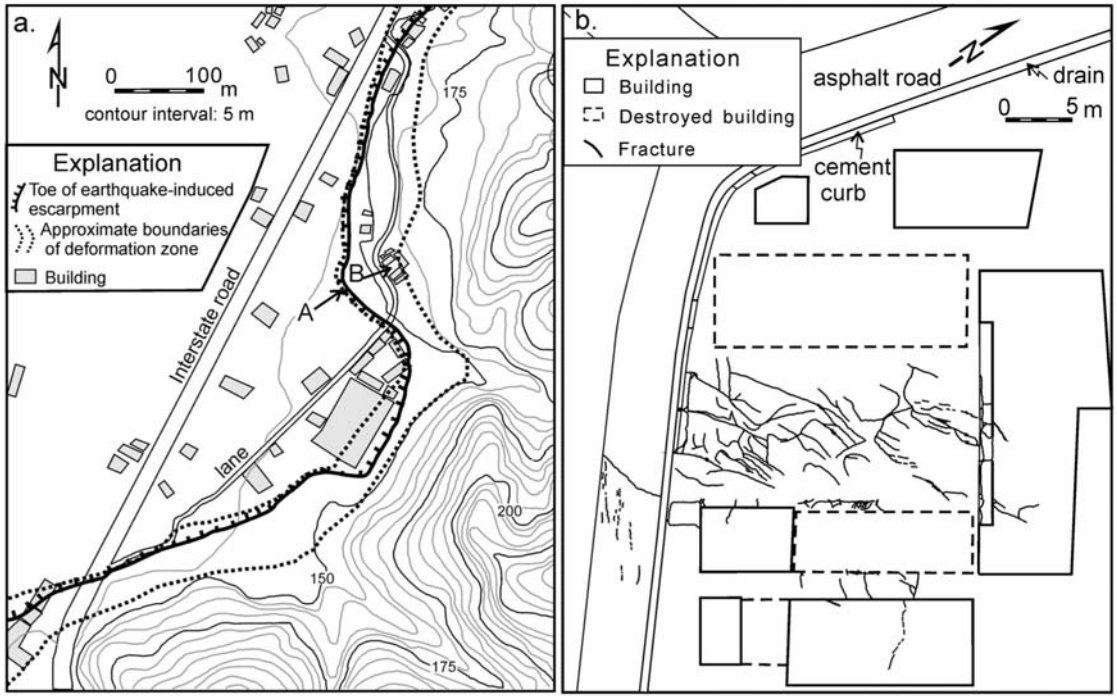

Figure 10. Deformation zone in Tanliwun area near Chushan, central Taiwan. (a) The east (right) side of the escarpment was lifted up 1 to 2 m relative to the west side. Point A is site of Chushan trench, through which the main rupture passes. Point B is Shanhu Yuan that exposes the deformation zone in the hanging wall. (b) Setting and traces of larger fractures in the Shanhu Yuan (point B, Figure 10a). The courtyard and road were paved with asphalt. The kinematics of all the fractures in the asphalt were a result of horizontal compression in the NE-SW direction as well as sufficient horizontal tension NW-SE to produce tension cracks.

to intersect the fault [*Chen et al.*, 2007]. The dip angle of the fault at Tanliwun is consistent with the dip angle of the Chi-Chi fault over a broad area, generally 20° to 30° E. The width ratios, w_{HW}/w_{FW}, estimated according to field observations is highly variable, but appears to be generally large because the main rupture is near the leading edge of the deformation zone (Figure 10a). Other dimensional parameters for the fault were a fault length of 80 km and a fault width W_f = 30 km according to a seismic study of *Kao and Chen* [2000] (Table 6). The width of the deformation zone at Tanliwun ranges from w = 50 to 100 m (Figure 10). The amount of reverse slip near the ground surface in Chushan trench and at depth was about 3 m [*Huang*, 2006; *Johnson et al.*, 2001].

[60] We select values for two parameters in order to simulate the deformation zone at Tanliwun: the slip on the fault is 3 m and the dip angle of the fault is 24° E. Only one parameter, the critical yield condition, $(II^e_{\varepsilon'})_c$, needs to be adjusted in order to analyze the shear zone. Examination of Figure 7a indicates that for a dip of 24° the width ratio should be w_{HW}/w_{FW} = 5. We use Figure 7c, to relate the exponent, n, of $(II^e_{\varepsilon'})_c$ to the normalized width of the deformation zone and the fault dip angle. The width of the deformation zone ranges between 72 and 78 m so the normalized width ranges between w/S = 24 and 26. Examining Figure 7c, we see that for a fault dip angle of 24°, the exponent of $(II^e_{\varepsilon'})_c$ should range from about −3.8 to −3.9. Thus, we estimate $10^{-3.8} \leq (II^e_{\varepsilon'})_c \leq 10^{-3.9}$ so that value would be $(II^e_{\varepsilon'})_c \cdot 1.3$ to 1.6×10^{-4}, which corresponds to a representative critical strain of $1.1 \times 10^{-2} \leq {}_r\varepsilon'_c \leq 1.3 \times 10^{-2}$ (Table 3). This critical strain is close to the values determined at Granada Hills and landslide debris at Aspen Grove (Table 1).

Table 6. Values of Parameters for Tanliwun Deformation Zone

Parameter	Measured	Assumed	Varied	Calculated
Fault width, W_f (m)		Yes, 30×10^3[a]		
Width ratio, w_{HW}/w_{FW}	large[b]			5
Fault dip, θ (deg)	20 E to 30 E[a], 24 E[b,c]	Yes, 24 E		
Width of deformation zone, w (m)	50 to 100[b]			72 to 78
Slip, S (m)	3[b,d]	Yes, 3		
Normalized width of deformation zone, w/S				24 to 26
Exponent in value of yield condition, n (10^n)			Yes	−3.8 to −3.9

[a] *Kao and Chen* [2000].
[b] *Huang* [2006].
[c] *Chen et el.* [2007].
[d] *Johnson et al.* [2001].

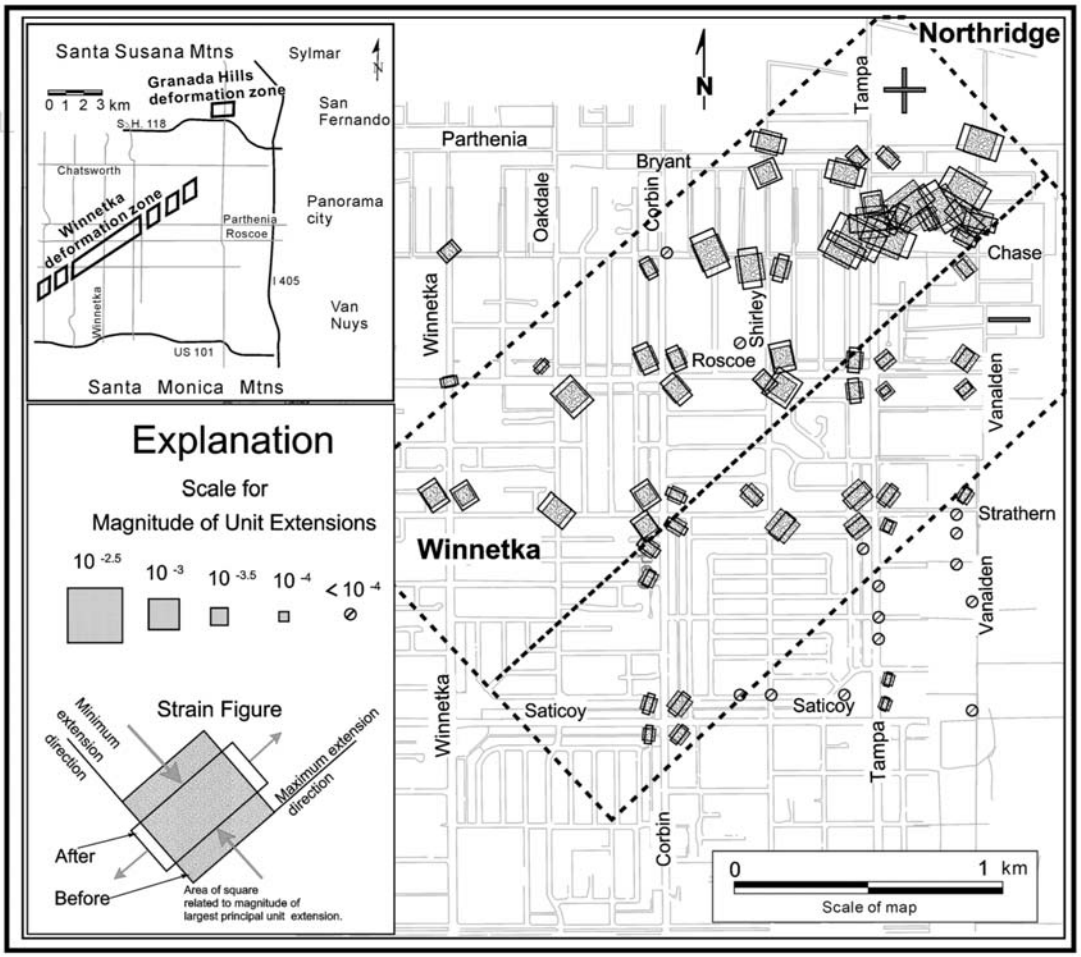

Figure 11. The extension belt (upper left) and shortening belt (lower right) in the part of the Winnetka deformation zone where strains were measured completely [after *Johnson et al.*, 1996a, Figure 9]. The zone of measureable strains trends NE-SW and is about 1.5 km wide.

[61] According to field observation, the width of the deformation zone ranges from 50 to 100 m, so the expected value is 75 m. We obtain 72 to 78 m from a numerical simulation (Table 6), which is within the range of observed values. According to the numerical solution, the deformation zone at Tanliwun began to form when the tip of the slipped patch on the fault was at a distance of $W_f - W_{ts}$ = 107 m from the fault tip at the ground surface to the tip of the slipped patch at depth, as measured along the fault. The tip of the slipped patch was at a depth of D_{ts} = 44 m beneath the ground and 98 m east of the ultimate surface rupture at the trench (Table 4). The tip of the slipped patch was perhaps 50 m below and 30 or 50 m east of the Shanhu Yuan (Figure 10b) at that time. This result is consistent with the observation of E-W shortening in the yard of the Shanhu Yuan (Figure 10b), which was probably a manifestation of the deformation zone.

7.4. Blind, Normal Coactive Fault at Northridge, California

[62] The Winnetka deformation belts, which formed during the 1994 Northridge, California earthquake in Los Angeles, was a two-ply zone of relatively high strains consisting of a belt of horizontal extension on one side and a belt of horizontal shortening on the other, each belt roughly 500 m wide, centered on Winnetka and extending at least 4.5 km in the NE-SW direction. The deformation belts are not attributed to the reactivation of the Northridge thrust [*Huftile and Yeats*, 1996] but a blind fault in its hanging wall. It is likely that the belts extended into areas of relatively high damage to buildings in the southwest in Canoga Park and in the northeast in Northridge and California State University at Northridge, in which case the belts could have been 9 km long [*Cruikshank et al.*, 1996].

[63] The Winnetka deformation belts were detected in unprecedented detail by resurveys of subsurface monuments before and after the 1994 earthquake. The relative horizontal positions of monuments at most street intersections and in places between street intersections had been measured throughout Los Angeles after the 1971 San Fernando earthquake sequence. In cooperation with the city of Los Angeles, *Cruikshank et al.* [1996] hired the city to resurvey the lengths of street segments in part of the Winnetka area in 1995 in order to establish the NW and SE boundaries of the Winnetka deformation belts. In the NE part of the Winnetka deformation zone, the city surveyed lengths of street segments and angles between intersecting streets (Figure 11) so that *Cruikshank et al.* [1996] could compute strains and

Table 7. Values of Parameters for Winnetka Deformation Zone

Parameter	Measured	Assumed	Adjusted	Calculated
Fault width, W_f (m)		Yes, 3000[a]		
Slip, S (m)		Yes, 1.6[b]		
Total width strain belts, w (m)	1540 to 1580[c]			
Normalized width of belts, w/S	963 to 988			
Normalized Depth to fault tip, D_{ts}/S			Yes	220 to 230
Depth to fault tip, D_{ts} (m)				350 to 370
Width ratio, w_E/w_S	1.6 to 2[c]			
Fault dip, θ (deg)			Yes	50 to 58 S

[a] *Huftile and Yeats* [1996].
[b] The size of an anomaly in the differential vertical displacement map near Northridge [*Cruikshank et al.*, 1996, Figure 2] is 0.6 to 0.8 m. The slip therefore was probably on the order of 1.2 to 1.6 m.
[c] *Cruikshank et al.* [1996].

investigate the internal structure of the deformation belts. The strains are shown via strain figures in Figure 11. The survey data and computational methods are presented by *Johnson et al.* [1996a] and *Cruikshank et al.* [1996].

[64] The strain figures are largely segregated into different rectangular belts within the deformation zone. Most of the strain figures that show extension roughly normal to the long sides of the rectangular belts are in the upper left belt shown in Figure 11; they generally show NW-SE extension. Most of the plots that show shortening in that same direction are in the lower right belt in Figure 11; they generally show NW-SE shortening.

[65] The ground rupture and damage to the infrastructure correlated in kind and position with the belts of horizontal extension and shortening within the deformation belts but no surface rupture could be identified [*Cruikshank et al.*, 1996]. Although predominantly tension fractures were mapped in the NE end of the Winnetka extension deformation belt, there were scant signs of damage to streets or sidewalks within the shortening deformation belt. The extensions measured in the NE belt of the Winnetka zone, on either side of Tampa Avenue and between Parthenia and Chase streets (Figure 11), were apparently large enough, on the order of 10^{-3} to 1.6×10^{-3}, to fracture concrete and soils. The fractured ground in the NE part of the deformation zone, though, must have been brittle, fracturing at relatively small strains. The damage in the belt of shortening was small. The magnitudes of the larger strains were on the order of $|-0.3 \times 10^{-3}|$, one third to one fifth the magnitude of the strains in the belt of extension.

[66] The strains in the Winnetka area were generally smaller than the strains in the Granada Hills area (locations shown in Figure 11); the damage was much higher in the Granada Hills area also [*Johnson et al.*, 1996a]. These observations suggest that the deformation in Winnetka area could have been largely elastic and thus it is unclear whether a classic deformation belt formed at Winnetka. It is unclear whether there were permanent ground deformations outside the NE part of the Winnetka zone, near intersections of Parthenia and Chase streets with Tampa and Vanalden streets (Figure 11). Not only are we uncertain whether the Winnetka zone is a classic deformation zone, like those at Kaynaşlı, Chung-Cheng Park and Tanliwun, but we found no trace of a fault rupturing the ground surface, suggesting that if the pattern of strains is a result of faulting, as we suppose, the fault must be blind.

[67] Following are the salient features of the deformation belts at Winnetka:

[68] 1. The deformation belts are defined primarily by elevated strains and secondarily by damage to sidewalks, roads, houses and utilities. The width of the zone of measurable strains is 1.5 to 1.6 km at Winnetka.

[69] 2. The strain figures show that the directions of principal extensions are parallel and normal to the walls of the deformation belts.

[70] 3. One of the striking characteristics of parallel belts of the Winnetka zone of strain figures, therefore, is that the maximum extension in the extension belt is parallel to the maximum shortening in the immediately adjacent shortening belt (Figure 11).

[71] 4. The Winnetka zone contains a belt of NW-SE extension with a width of $w_E = 0.94$ to 1.05 km and a belt of NW-SE shortening with a width of $w_S = 0.60$ to 0.53 km. Thus, it is not due to a strike-slip blind fault but rather to a normal or a reverse blind fault.

[72] 5. If the strains that we measured in the shortening belt were permanent, we would estimate that the critical yield value would have to be unusually small, approximately, $(II^e_{\varepsilon'})_c \cong 10^{-7}$ (an equivalent critical strain of -3×10^{-4}). The strains are also unusually small in the extension belt, except in the NE part of the extension belt, where the ground was clearly fractured. If that area had permanent deformation, critical values of the deviatoric strain invariant were rather low $(II^e_{\varepsilon'})_c \cong 10^{-6}$ to 2.5×10^{-6}. This range is still low but is more nearly consistent with the values we have estimated or calculated elsewhere (Table 1).

[73] The training simulations (Figures 4, 5, and 6) provide all the clues needed to determine that the pattern at Winnetka is expected for a blind, normal, dip-slip fault. Figure 4 shows strain patterns associated with blind strike-slip and dip-slip faults. According to Figure 4 (right), (1) for a dip-slip fault, the strains normal to the strike of the fault change sign across the vertical projection of the tip of the slipped patch to the ground surface; (2) the strain is essentially zero at the vertical projection of the tip of the slipped patch; (3) the strains are the same sense as the fault (i.e., extension for a normal fault) in front of the vertical projection of the tip of the slipped patch; they are opposite behind the projection, and (4) the largest strain magnitude is in the belt of shortening for a reverse fault and, by analogy, in the belt of extension for a normal fault. The first three features are invalid when the vertical projection of the tip of the slipped patch is within the zone of permanent deformation as shown, for example, in Figures 4c (right) and 4d (right). The permanent strains change the features. According to Figures 5 and 6, the strain with largest magnitude is a shortening for the reverse fault and an extension for the normal fault. The dip direction of the blind fault is also determined by the ratio, w_S/w_E, where w_S is the width of the shortening belt and w_E is the width of the extension belt. If the ratio is <1, the fault is a normal fault. If the ratio is >1, the fault is a reverse fault (Figure 4b, right).

[74] In order to analyze the deformation zone at Winnetka we assume that there is a "blind" dip-slip fault, normal or reverse, the slip on which terminated below the Winnetka deformation zone. The fault slip is fixed for the analysis: it

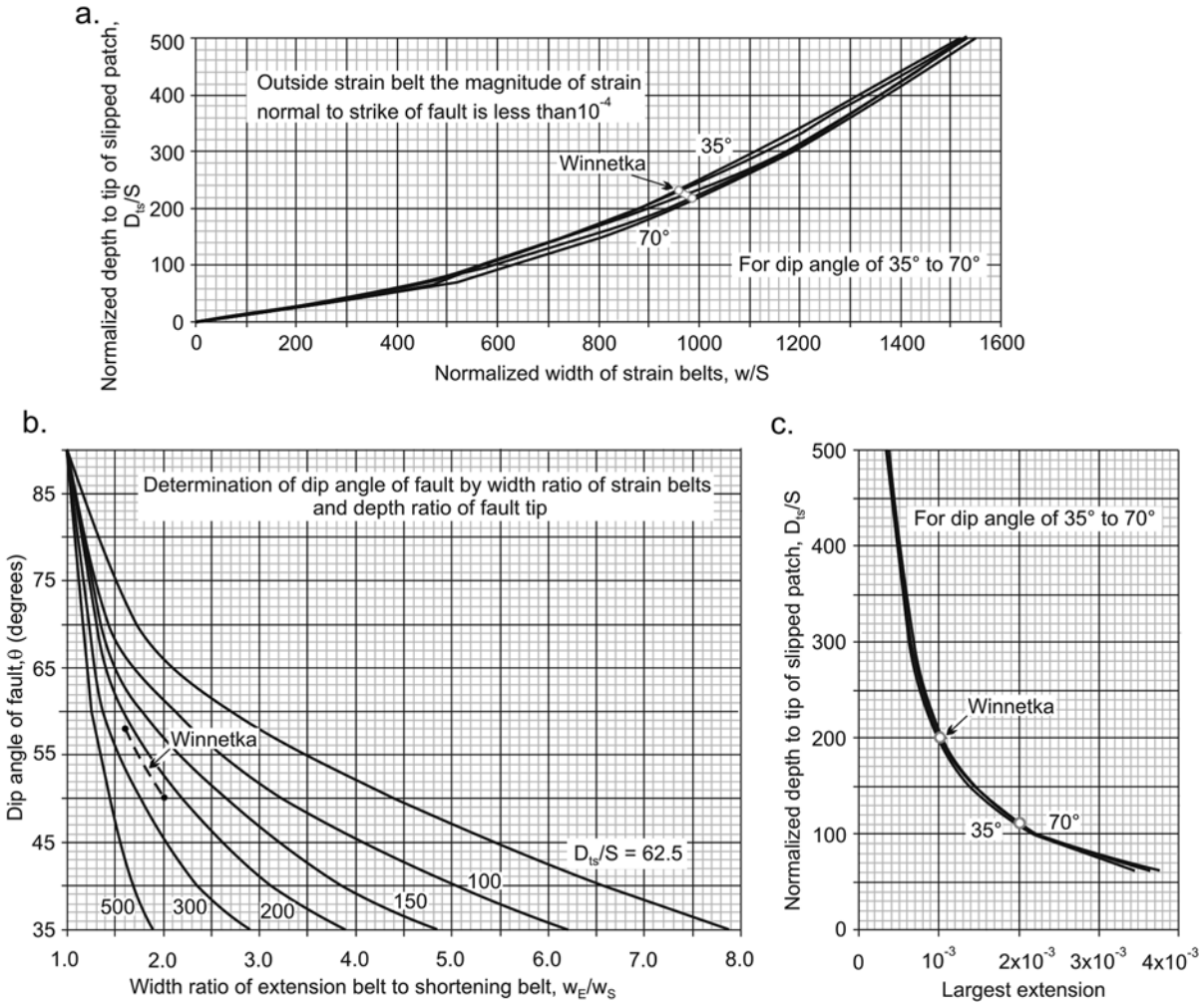

Figure 12. Analytical diagrams used to determine depth to tip of the slipped patch on blind fault and dip angle of the blind fault for Winnetka strain belts. The slip of the blind fault is 1.6 m. The width of the zone of measureable strains is 1.5 to 1.6 km at Winnetka. (a) Relation between normalized depth to tip of the slipped patch, D_{ts}/S, where S is slip, to the normalized total width of the pair of strain belts, w/S, for blind fault dips ranging from 35° to 70°; w/S of Winnetka strain belts ranges between 963 and 988. (b) Relation between dip angle of fault and width ratio of extension belt to shortening belt, w_E/w_S, for normalized values of depth to tip of the slipped patch ranging from about 63 to 500. D_{ts}/S of Winnetka strain belts ranges between 50 and 58, and w_E/w_S ranges between 1.6 and 2. (c) Relation between D_{ts}/S and the magnitude of the largest extension in the extension belt. A check on the results for the normalized depth to the tip of the slipped patch, D_{ts}/S. Large extension of Winnetka strain belts is on the order to 10^{-3}, perhaps as large as 2×10^{-3}.

is assumed to be S = 1.6 m (for reason noted in Table 7). The fault width is also fixed for the analysis: it is assumed to be W_f = 3 km in width. The estimate of the width is weak, based only on the width of the Chatsworth Reservoir normal fault in San Fernando Valley [*Huftile and Yeats*, 1996, Figure 2a]. Whether the blind fault is a normal fault or a reverse fault is determined by the ratio w_E/w_S. Clearly, the fault beneath the Winnetka deformation zone is a normal fault. Since the wide extension belt is NW of the narrow shortening belt, the fault is normal and the downthrown side is on the SE side of the fault. We have used an analysis of a blind rectangular dislocation/fault in an elastic medium in order to determine the parameters. We cannot use the analysis for the deformation zone in this case, because the strains are generally too small for there to have been much permanent deformation, except in the NE end of the Winnetka extension belt (Figure 11).

[75] Thus, we use the parameters already defined in order to make analytical diagrams. In keeping with the accuracy of strain measurements by surveying, we assume that the edges of the strain belts are defined by a strain of 10^{-4}. This is the strain in the direction normal to the boundary between the shortening and extension belt; at Winnetka, the normal strains trend NE. In principal, the solution provides a way of determining the depth to the tip of the slipped patch on the fault, D_{ts}. Figure 12a shows the relation between normalized depth to the tip of the slipped patch, D_{ts}/S, where S is the slip, to the normalized total width of the pair of strain belts, w/S. The relations are slightly different for different dip angles of the fault, as indicated by the bundle of curves for

dips ranging from 35° to 70°, but the differences are small. The values of measurements and the solution for the depth to the tip of the slipped patch of the blind fault are shown in Table 7. We see that the depth to the upper end of the blind fault was $D_{ts} \cong 350$ to 370 m at the time the Winnetka strain belts formed. Using this estimate of $D_{ts}/S = 220$ to 230 and measurements of the width of the extension belt, w_E, to the shortening belt, w_S, to form the ratio, $w_E/w_S = 1.6$ to 2, we use Figure 12b to determine that the dip angle of the fault was approximately, $\theta \cong 50°$ to 58°. In this way, the values were obtained for the two unknown parameters, D_{ts}, the depth to the upper end of the blind fault and θ, the dip angle of the fault.

[76] Figure 12c shows another way of estimating the normalized depth to the tip of the slipped patch D_{ts}/S, in terms of the maximum strain, normal to the walls of the belt, within the extension belt. With Figure 12c we determine that since the largest strain in the extension belt, outside the NE part of the belt where ground fracturing occurred, is on the order to 10^{-3}, perhaps as large as 2×10^{-3}, the depth ratio of the tip of the slipped patch should be approximately $D_{ts}/S = 200$ to perhaps as low as 110. We estimated 220 to 230 by the first method. The two methods give similar results.

8. Discussion and Conclusion

[77] The theoretical model used to analyze strike-slip and reverse-slip deformation zones at Kaynaşlı, Turkey, and Chi-Chi, Taiwan, is based on the assumption of permanent (elastic-plastic) deformation at the ground surface and above the fault at depth as slip propagates along the fault toward the ground surface. The theory suggests that the width of the deformation zone and the position of fault rupture within the deformation zone are determined by parameters including the material properties of the ground near the fault, geometric properties of the fault and the amount and sense of slip of the fault. Although the geometric variables in the theory are clearly relevant to the phenomenon, the material properties assumed for the ground by the theory are so elementary that they may be inadequate to describe the phenomenon. Besides elastic properties, we characterize the permanent yielding of the ground in terms of a single parameter, identified as an exponent, n, or a critical second invariant of elastic strain, $(II^e_{\varepsilon'})_c$. The theoretical model, although clearly incomplete and somewhat "cobbled" together, is our most recent attempt to quantitatively study and, at some level, to understand why deformation zones should form along earthquake ruptures and how their geometric properties might be interrelated.

[78] According to the analysis of the deformation zone mechanism, the ratio of widths of deformation zone in hanging wall and footwall of dipping faults, w_{HW}/w_{FW}, is largely controlled by fault dip angle and the kind of fault: the relations are different for strike-slip and dip-slip faults (Figure 7a). The relations are independent of the value of the yield condition, $(II^e_{\varepsilon'})_c$. Thus, if one knows the dip angle and type of a fault, the model will determine a width ratio, w_{HW}/w_{FW}. Or, if one knows the width ratio, the model will determine a dip angle for the fault. The analysis indicates that total width of the deformation zone, $w = w_{HW} + w_{FW}$, normalized with fault slip during the earthquake, w/S, is determined by two parameters, the dip angle, θ, and the exponent, n, of the yield condition, $(II^e_{\varepsilon'})_c$, as well as whether the fault is dip slip (Figure 7c) or strike slip (Figure 7b).

[79] We note that there are some simplifications that we make in our model, such as constant fault slip on patches, infinite fault length and constant rheology, that could significantly affect the analyses of real cases. A group of researchers [i.e., *Freymueller et al.*, 1994; *Johnson et al.*, 2001, *Fialko et al.*, 2005] have shown that coseismic slips are nonuniform on faults and commonly vary with depth. On the one hand, our assumption of uniform slip is inconsistent with their findings. On the other hand, we have learned from our case studies that the deformation zones start to develop when slip has propagated up to shallow depths, smaller than 0.5 km, indicating that it is the slip on the part of the fault at shallow depth that is crucial in the formation of deformation zones. Thus, other things being equal, an assumption of uniform slip may be acceptable in an analysis of a deformation zone because it forms at the ground surface. The simplification of infinite fault length for our model excludes a possible effect which results from lateral propagation of slip. Strike-slip faults propagate laterally, in mode II and mode III, after nucleating at depth [e.g., *Scholz*, 2002]. Near the ground surface, however, we have noted that strike-slip faults in landslides and earthquake ruptures tend to propagate in mode III, that is, toward the ground surface. In our simplified analysis, we assume that the effect of propagation of slip in mode II near the ground surface on the formation of the deformation zone is insignificant. However, due to this simplification, our model cannot apply to deformation zones which occur in the regions close to the ends of fault traces. It is important to recognize that there will be variations in rheology of the ground through which the fault slip propagates and that these variations can significantly affect the formation of deformation zones. *Savage* [1987, 1998] and *Schmalzle et al.* [2006] have analyzed effects of layering and changes in properties laterally on deformation associated with fault propagation, but such analyses are beyond the scope of our study.

[80] We have applied the theoretical model to deformation zones along the strike-slip, Düzce-Bolu fault at Kaynaşlı, Turkey, and two thrust deformation zones of quite different widths along the Chi-Chi earthquake rupture at Chung-Cheng Park and Tanliwun, Taiwan. The parameters are compared in Table 3. Quantitative analyses of the deformation zones illustrate how one uses the theoretical model to characterize the deformation zones mechanically and show that the theoretical values of parameters agree quite well with strain measurements, dip angles and other data determined from geophysical and geological studies. The theoretical model also helps one to interpret the Winnetka deformation belts that formed above the Winnetka blind fault during the 1994 Northridge earthquake (Table 7).

[81] We have some information about the internal consistency of the parameters identified with the theory, particularly the parameters of width ratio, w_{HW}/w_{FW}, and dip angle of the fault. For example, theoretically the width ratio, w_{HW}/w_{FW}, is related only to the fault dip angle, θ. We have an internal check with these variables, then, if they are both measured. The dip angle was determined indepen-

dently with GPS measurements and dislocation theory by *Bürgmann et al.* [2002] to be on average, $\theta = 54°$ N for the entire Düzce-Bolu fault. With the deformation zone analysis, we used the observed width ratio, $w_{HW}/w_{FW} = 6$ to determine that the dip angle of the Düzce-Bolu fault at Kaynaşlı was $\theta = 44°$ N (Table 2). The values for dip angle are remarkably close, since Bürgmann's estimate was for the whole length (40 km) and width (20 km) of the fault whereas ours is for a relatively short segment of the fault. Difference in scales of the analyses are suggested by the fact that our results indicate that the deformation zone at Kaynaşlı is a result of a highly localized process, that the zone started to form when the tip of the slipped patch was only about 74 m beneath the ground surface. Accepting the dip angles of 20 to 30° determined for a large part of the fault by *Kao and Chen* [2000], the lower end of their dip measurements are close to our computed value of about 17° E (Table 5). Thus, the width ratio and dip angle were both known moderately well at Chung-Cheng Park, so one can conclude that the dip parameter is internally consistent with the width ratio and Chung-Cheng Park as well as at Kaynaşlı.

[82] We have only weak checks of consistency for other parameters because they are related, theoretically, through the yield condition, $(II^e_{\varepsilon'})_c$, which is rather poorly controlled. Indeed, the only values of $(II^e_{\varepsilon'})_c$ that we have computed independently are presented in Table 1, for landslide debris, concrete and asphalt, and a very brittle granite. Theoretically, the yield condition, $(II^e_{\varepsilon'})_c$, is determined by the dip angle, θ (or width ratio, w_{HW}/w_{FW}), the normalized width, w/S, of the deformation zone and the type of fault in Figures 7b and 7c. The only check we have on internal consistency of these variables comes from the values of the yield condition, $(II^e_{\varepsilon'})_c$. Ignoring the extremes in Table 1, the range of values is $10^{-4} \leq (II^e_{\varepsilon'})_c \leq 10^{-3}$. Comparing this range of the yield values with the range of yield values calculated from the deformation zones, $10^{-4.4} \leq (II^e_{\varepsilon'})_c \leq 10^{-3.8}$ (Table 3), we see that calculated values for the deformation zones are somewhat smaller than the range estimated from field and laboratory observations. Even though the estimated values of the yield condition, $(II^e_{\varepsilon'})_c$, might appear to be consistent, we would maintain that the parameter $(II^e_{\varepsilon'})_c$ must be considered to be merely an empirical "constant."

[83] Thus, we conclude that one needs to be able to understand how deformation zones form so that their characteristics, including total width, partitioning of the distortion on either side of the fault trace and the amount of distortion to be expected at various places within the zone, can be estimated. We have posited in this paper a credible mechanism of formation of a deformation zone based on observations of several examples in the field, a few of which are described herein. The mechanism suggested here appears to lead to a plausible explanation for many of the features we have observed in deformation zones. More important, however, analysis of the mechanism suggests a set of parameters that appear to characterize many features of deformation zones. Knowledge of the characteristic parameters, such as dip of the fault, the sense and amount of slip on the fault, the width of the deformation zone, and an estimate of the yield criterion, should help one predict the widths of the deformation zone in the hanging wall and footwall of the fault, the depth of the tip of the slipped patch at which the deformation zone will begin to form. Knowledge of the mechanism, plus practical knowledge from field study of deformation zones associated with various kinds of fault that have ruptured to the ground surface, therefore, guide the observations, measurements and calculations needed to characterize what a deformation zone will most likely be like along a fault in an unfamiliar area.

[84] **Acknowledgments.** This research was supported by the Department of Earth and Atmospheric Sciences, Purdue University. It is a contribution of the Institute of Earth Sciences, Academia Sinica, IESAS1389.

References

Akyüz, H. S., R. Hartleb, A. Barka, E. Altunel, G. Sunal, B. Meyer, and R. Armijo (2002), Surface rupture and slip distribution of the 12 November 1999 Düzce earthquake (M 7.1), North Anatolian Fault, Bolu, Turkey, *Bull. Seismol. Soc. Am.*, *92*(1), 61–66, doi:10.1785/0120000840.

Atkinson, B. K. (1987), *Fracture Mechanics of Rock*, 534 pp., Academic, London.

Aydin, A., A. M. Johnson, and R. Fleming (1992), Right-lateral/reverse surface rupturing along the San Andreas and Sargent fault zones during the October 17, 1989 Loma Prieta, California, earthquake, *Geology*, *20*, 1063–1067, doi:10.1130/0091-7613(1992)020<1063:RLRSRA>2.3.CO;2.

Baum, R. L., A. M. Johnson, and R. W. Fleming (1988), Measurement of slope deformation using quadrilaterals, *U.S. Geol. Surv. Bull. 1842B*, 23 pp.

Baum, R. L., R. W. Fleming, and A. M. Johnson (1993), Kinematics of the Aspen Grove landslide, Ephraim Canyon, central Utah, *U.S. Geol. Surv. Bull. 1842F*, 34 pp.

Bürgmann, R., M. E. Ayhan, E. J. Fielding, T. J. Wright, S. McClusky, B. Aktug, C. Demir, O. Lenk, and A. Türkezer (2002), Deformation during the 12 November 1999 Düzce, Turkey, earthquake, from GPS and InSAR data, *Bull. Seismol. Soc. Am.*, *92*(1), 161–171, doi:10.1785/0120000834.

Chen, W. S., et al. (2007), Late Holocene paleoseismicity of the southern part of the Chelungpu Fault in central Taiwan: Evidence from the Chushan excavation site, *Bull. Seismol. Soc. Am.*, *97*(1b), 1–13, doi:10.1785/0120050161.

Cruikshank, K. M., A. M. Johnson, R. W. Fleming, and R. Jones (1996), Winnetka deformation zone: Surface expression of coactive slip on a blind fault during the Northridge earthquake sequence, California, *U.S. Geol. Surv. Open File Rep. 96–698*, 70 pp.

Dong, J. J., C. D. Wang, C. T. Lee, J. J. Liao, and Y. W. Pan (2004), The influence of surface ruptures on building damage in the 1999 Chi-Chi earthquake: A case study in Fengyuan City, *Eng. Geol.*, *71*, 157–179, doi:10.1016/S0013-7952(03)00131-5.

Fialko, Y., D. Sandwell, M. Simons, and P. Rosen (2005), Three-dimensional deformation caused by the Bam, Iran, earthquake and the origin of shallow slip deficit, *Nature*, *435*, 295–299, doi:10.1038/nature03425.

Fleming, R. W., and A. M. Johnson (1989), Structures associated with strike-slip faults that bound landslide elements, *Eng. Geol.*, *27*, 39–114, doi:10.1016/0013-7952(89)90031-8.

Fleming, R. W., and A. M. Johnson (1997), Growth of a tectonic ridge, *Geology*, *25*, 323–326, doi:10.1130/0091-7613(1997)025<0323:GOATRD>2.3.CO;2.

Fleming, R. W., A. M. Johnson, and J. A. Messerich (1997), Growth of a tectonic ridge, *U.S. Geol. Surv. Open File Rep. 97–153*, 94 pp., 6 plates.

Fleming, R. W., J. A. Messerich, and K. M. Cruikshank (1998), Fractures along a portion of the Emerson fault zone related to the 1992 Landers, California, earthquake: Evidence for the Galway Lake Road rotated block, *Geol. Soc. Am. Map Chart Ser.*, *MCH082*, scale 1:3000.

Freymueller, J., N. E. King, and P. Segall (1994), The co-seismic slip distribution of the Landers earthquake, *Bull. Seismol. Soc. Am.*, *84*(3), 646–659.

Gamond, J. F. (1983), Displacement features associated with fault zones: A comparison between observed examples and experimental models, *J. Struct. Geol.*, *5*, 33–45, doi:10.1016/0191-8141(83)90005-6.

Gilbert, G. K. (1907), The earthquake as a natural phenomenon, in *The San Francisco Earthquake and Fire*, *U.S. Geol. Surv. Bull*, *324*, 1–13.

Gür, T. (2004), Earthquake effects on articulated structures location in fault rupture zones, Ph.D. dissertation, 191 pp., Purdue Univ., West Lafayette, Indiana, May.

Huang, W. J. (2006), Deformation at the leading edge of thrust faults, Ph.D. dissertation, 435 pp., Purdue Univ., West Lafayette, Indiana, July.

Huftile, G. J., and R. S. Yeats (1996), Deformation rates across the Placerita (Northridge Mw = 6.7 aftershock zone) and Hopper Canyon segments of the western transverse ranges deformation belt, *Bull. Seismol. Soc. Am.*, *86*(1B), S3–S18.

Johnson, A. M., R. W. Fleming, and K. M. Cruikshank (1993), Broad belts of shear zones as the common form of surface rupture produced by the 28 June 1992 Landers, California, earthquake, *U.S. Geol. Surv. Open File Rep. 93–348*, 61 pp.

Johnson, A. M., K. M. Cruikshank, and R. W. Fleming (1994a), Borrego Mountain, Loma Prieta, Landers, Northridge: Simply earthquakes or seismostructural events?, *Eos Trans. AGU*, *75*(16), Spring Meet. Suppl., 343.

Johnson, A. M., R. W. Fleming, and K. M. Cruikshank (1994b), Shear zones formed along long, straight traces of fault zones during the 28 June 1992 Landers, California, earthquake, *Bull. Seismol. Soc. Am.*, *84*(3), 499–510.

Johnson, A. M., R. W. Fleming, K. M. Cruikshank, and R. F. Packard (1996a), Coactive fault of the Northridge earthquake–Granada Hills area, California, *U.S. Geol. Surv. Open File Rep. 96–523*, 66 pp.

Johnson, A. M., R. W. Fleming, S. Y. Martosudarmo, N. A. Johnson, K. M. Johnson, and W. Wei (1996b), Analecta of structures formed along strike-slip fault zones during 28 June 1992 Landers, California earthquake sequence, *U.S. Geol. Surv. Open File Rep. 97-97-94*, 59 pp., 10 plates.

Johnson, A. M., R. W. Fleming, K. M. Cruikshank, S. Y. Martosudarmo, N. A. Johnson, K. M. Johnson, and W. Wei (1997), Analecta of structures formed during the 28 June 1992 Landers–Big Bear, California, earthquake sequence, *U.S. Geol. Surv. Open File Report 97-94*, 59 pp.

Johnson, K. M., Y. J. Hsu, P. Segall, and S. B. Yu (2001), Fault geometry and slip distribution of the 1999 Chi-Chi, Taiwan earthquake imaged from inversion of GPS data, *Geophys. Res. Lett.*, *28*(11), 2285–2288, doi:10.1029/2000GL012761.

Johnson, A. M., K. M. Johnson, J. Durdella, M. Sözen, and T. Gür (2002), An emendation of elastic rebound theory: Main rupture and adjacent belt of right-lateral distortion detected by viaduct at Kaynasli, Turkey 12 November 1999 Duzce earthquake, *J. Seismol.*, *6*, 329–346, doi:10.1023/A:1020031324622.

Kao, H., and W. P. Chen (2000), The Chi-Chi earthquake sequence: Active, out-of-sequence thrust faulting in Taiwan, *Science*, *288*, 2346–2349, doi:10.1126/science.288.5475.2346.

Kelson, K. I., K. H. Kang, W. D. Page, C. T. Lee, and L. S. Cluff (2001), Representative styles of deformation along the Chelungpu fault from the 1999 Chi-Chi (Taiwan) earthquake: Geomorphic characteristics and responses of man-made structures, *Bull. Seismol. Soc. Am.*, *91*(5), 930–952, doi:10.1785/0120000741.

Lawson, A. C. (1908), California earthquake of April 18, 1906: Report of the State Earthquake Investigations Commission, *Carnegie Inst. Washington Publ.*, *87*(1), 451 pp.

Lazarte, C. A., J. D. Bray, A. M. Johnson, and R. E. Lemmer (1994), Surface breakage of the 1992 Landers earthquake and its effects on structures, *Bull. Seismol. Soc. Am.*, *84*(3), 547–561.

Lee, Y. H., M. L. Hsieh, S. D. Lu, T. S. Shih, W. Y. Wu, Y. Sugiyama, T. Azuma, and Y. Kariya (2003), Slip vectors of the rupture of the 1999 Chi-Chi earthquake, western Taiwan, *J. Struct. Geol.*, *25*, 1917–1931, doi:10.1016/S0191-8141(03)00039-7.

Martosudarmo, S. Y., A. M. Johnson, and R. W. Fleming (1996), Ground fracturing on the southern end of Summit Ridge caused by the October 17, 1989 Loma Prieta, California earthquake, *U.S. Geol. Surv. Open File Rep. 97–129*, 43 pp., 5 plates.

Peng, S., and A. M. Johnson (1972), Crack growth and faulting in cylindrical specimens of Chelmsford granite, *Int. J. Rock Mech. Min. Sci.*, *9*, 37–86, doi:10.1016/0148-9062(72)90050-2.

Reid, H. F. (1910), Report of the State Earthquake Investigation Commission, II: The mechanics of the earthquake, 192 pp., Carnegie Inst. of Washington, Washington, D. C.

Savage, J. C. (1987), Effect of crustal layering upon dislocation modeling, *J. Geophys. Res.*, *92*(B10), 10,595–10,600, doi:10.1029/JB092iB10p10595.

Savage, J. C. (1998), Displacement field for an edge dislocation in a layered half-space, *J. Geophys. Res.*, *103*(B2), 2439–2446, doi:10.1029/97JB02562.

Schmalzle, G., T. Dixon, R. Malservisi, and R. Govers (2006), Strain accumulation across the Carrizo segment of the San Andreas Fault, California: Impact of laterally varying crustal properties, *J. Geophys. Res.*, *111*, B05403, doi:10.1029/2005JB003843.

Scholz, C. H. (2002), *The Mechanics of Earthquakes and Faulting*, Cambridge Univ. Press, New York.

Steinbrugge, K. V., E. E. Schader, and D. F. Moran (1973), Building Damage in San Fernando Valley, in *San Fernando, California, Earthquake of 9 February 1971*, edited by G. Oakeshott, *Calif. Div. Mines Geol. Bull.*, *196*, 323–368.

Taiwan Central Geological Survey (TCGS) (1999a), Surface ruptures along the Chelungpu fault during the Chi-Chi earthquake, Taiwan, map at scale , 1:25000, Central Geol. Surv., Minist. of Econ. Affairs, Taipei.

Taiwan Central Geological Survey (TCGS) (1999b), Report of the geological survey of the 1999 Chi-Chi earthquake (in Chinese), Central Geol. Surv., Minist. of Econ. Affairs, Taipei.

Umutlu, N., K. Koketsu, and C. Milkereit (2004), The rupture process during the 1999 Düzce, Turkey, earthquake from joint inversion of teleseismic and strong-motion data, *Tectonophysics*, *391*, 315–324, doi:10.1016/j.tecto.2004.07.019.

Vermilye, J. M., and C. H. Scholz (1998), The process zone: A microstructural view of fault growth, *J. Geophys. Res.*, *103*(B6), 12,333–12,237, doi:10.1029/98JB00957.

Yu, S. B., et al. (2001), Preseismic deformation and coseismic displacements associated with the 1999 Chi-Chi, Taiwan, earthquake, *Bull. Seismol. Soc. Am.*, *91*(5), 995–1012, doi:10.1785/0120000722.

W.-J. Huang, Institute of Earth Sciences, Academia Sinica, 128 Academia Rd., Sec. 2, Nankang Taipei 11529, Taiwan. (huang22@earth.sinica.edu.tw)

A. M. Johnson, Department of Earth and Atmospheric Sciences, Purdue University, 550 Stadium Mall Dr., West Lafayette, IN 47907, USA.